Metal Oxide Nanocluster-Modified TiO_2 as Solar Activated Photocatalyst Materials

Marco Fronzi,* Anna Iwaszuk, Aoife Lucid, and Michael Nolan†
Tyndall National Institute, University College Cork, Cork, Ireland
(Dated: October 9, 2015)

Abstract. In this review we describe our work on new TiO_2 based photocatalysts. The key concept in our work is to form new composite structures by the modification of rutile and anatase TiO_2 with nanoclusters of metals oxides and our density functional theory (DFT) level simulations are validated by experimental work synthesizing and characterizing surface modified TiO_2. We use DFT to show that nanoclusters of different metal oxides, TiO_2, SnO/SnO_2, PbO/PbO_2, NiO and CuO can be adsorbed at rutile and anatase surfaces and can induce red shifts in the absorption edge to enable visible light absorption which is the first key requirement for a practical photocatalyst. We furthermore determine the origin of the red shift and discuss the factors influencing this shift and the fate of excited electrons and holes. For p-block metal oxides we show how the oxidation state of Sn and Pb can be used to tune both the magnitude of the red shift and also its mechanism. Finally, aiming to make our models more realistic, we present some new results on the stability of water at rutile and anatase surfaces and the effect of water on oxygen vacancy formation and on nanocluster modification. These nanocluster-modified TiO_2 structures form the basis of a new class of photocatalysts which will be useful in oxidation reactions and with the suitable choice of nanocluster modified can be applied to CO_2 reduction.

PACS numbers: 68.35.bt, 68.43.Bc, 68.47.Jn, 85.50.Hp, 31.15.es

I. INTRODUCTION

TiO_2-based photocatalysts are of great interest as catalysts to decompose pollutants in air or water and for the oxidation of water, which arises from its strong ability to oxidise molecules. [1–5] In addition it is attractive due to its abundance in nature, high stability, and non-toxicity. [1–5] Unfortunately, rutile and anatase TiO_2 have band gaps larger than 3 eV, so that they only absorb UV-light which is ca. 3% of solar energy incident on the earth.[6, 7] Finding materials that absorb light in a wider wavelength range, particularly in the visible region of the electromagnetic spectrum (400 nm - 750 nm) will maximise use of the incident solar energy and is therefore the first key requirement in the efficient use of solar radiation. An important problem is that even if TiO_2 can be made visible-light active, this can come at the expense of its UV activity. We therefore seek to impart visible-light activity to TiO_2 but without reducing its UV-light activity. Visible light absorption can be induced in TiO_2, by doping TiO_2 with transition metal cations and non-metal anions or both (so-called co-doping) and this has been widely studied, with extensive reports and reviews of this important topic available [8–12] The role of doping is to modify the electronic structure of TiO_2, generally by introducing new states into

*Corresponding author
E-mail: marco.fronzi@tyndall.ie
†Corresponding author
E-mail: michael.nolan@tyndall.ie

the energy gap between the valence band and the conduction band. These tend to be in-gap electronic states which are usually localised.

Some key examples of doping of TiO_2 include: N-doping, where the N dopant is substituted onto an oxygen site, as proposed firstly by Asahi et al [13] and studied in extensive work by Di Valentin et al [14–16]. The general effect of N-doping is to introduce new dopant-derived states into the energy gap between the valence and conduction bands of TiO_2 which reduces the energy gap compared to undoped TiO_2.

Long and English have presented extensive studies of cation doped TiO_2 [17–19] and anion doped TiO_2 [20, 21] and studied the mechanism behind the reduction of the band gap of TiO_2 with doping. Nb-doping of TiO_2 has also been widely studied with DFT [22–24]. Umebayashi *et al.* [25] presented an extensive study of metal dopants in TiO_2 and found occupied levels in the TiO_2 energy gap with the electrons localised around the dopant. Regarding anionic dopants, Di Valentin et al. [26] have presented a study of anion doped anatase showing how the change in anion from B to C to N to F induces anion-derived electronic states in the TiO_2 energy gap for B-, C- and N-doping and reduced Ti^{3+} states in the gap for F-doping.

In the studies of doped TiO_2, a red shift in light absorption to longer wavelength can be achieved [10–12] but this can come at the cost of the new dopant-induced electronic states acting a trap sites that will enhance recombination of charge carriers, thus ultimately reducing activity. Co-doping [8, 9, 27, 28] can alleviate this issue by choosing metal and non-metal dopants that will passivate each other while still modifying the electronic structure to induce a red shift.

In addition, in some modified TiO_2 systems, while a visible-light response has been demonstrated, this can be at the cost of the UV-activity as described in work on Fe_2O_3-TiO_2 [29, 30] where reduced UV activity compared to unmodified TiO_2 is seen. Additionally in [31–33] there is a smaller UV enhancement compared to enhancement of visible light activity. This is relevant, as UV activity is still important in many applications, particularly for indoor applications. This problem arises as described above, where doping TiO_2 with an aliovalent metal cation results in formation of defect levels in the bulk that act as recombination centres. There are also other problems associated with doping, including reproducibility, stability and knowing if the dopant has been incorporated. Therefore ensuring effective charge separation is the next key requirement to achieve compatibility between visible- and UV- activities of TiO_2. Finally, while doping of TiO_2 is clearly an active and important field, it is not the subject of this review and we will refer the reader to the reviews in refs [10–12, 34].

In TiO_2-photo-catalyzed decomposition of organic pollutants, organic pollutants are oxidised by valence band (VB) holes and oxygen can be reduced by conduction band (CB) electrons [35]. Unfortunately, the driving force for the one-electron reduction of O_2 (the redox potential for $E^0(O_2/O_2^-) = -0.28$ V vs. standard hydrogen electrode, SHE) by electrons excited into the CB (CB energy = -0.53 V at pH 7) is small. Thus in order to to boost photocatalytic acivity of TiO_2 we seek to enhance the oxygen reduction reaction. TiO_2 photocatalysts are based on the anatase and rutile polymorphs of TiO_2; composites of rutile and anatase are also known, in particular Degussa P25,[36]. When we consider the photocatalytic decomposition of organics, the UV-activity of anatase is higher when compared to rutile. [37, 38] In visible light active TiO_2-based photocatalysts, the VB maximum should be raised up to induce visible light absorption, but not so high as to reduce the oxidising power of the holes and at the same time the position of the CB should not be modified downwards. For water splitting using TiO_2 based photocatalysts, the VB and CB levels must straddle the potentials for water oxidation and reduction, which places a further constraint on the choice of materials as photocatalysts.

A well studied and interesting approach for inducing visible-light activity in TiO_2 is to couple it with nano-structured metal chalcogenide semiconductors such as CdS, as described in refs [39, 40]. An interesting and

key feature of these metal chalcogenides is that their band edges (that determine the redox ability) can be varied over a wide range by controlling the particle size, that is the well known size quantization effect. This can enable efficient visible-light-induced interfacial electron transfer from the metal chalcogenide nano-particles (NPs, which absorb the visible light) to the TiO_2 semiconductor in a sensitization effect. These composite NP-TiO_2 structures are promising materials for visible-light photocatalysts but they will be unsuitable for environmental and aqueous applications because the oxidation ability of the VB-holes in metal sulfides is weak and the metal sulfide NPs undergo photo-irradiation induced dissolution. On the other hand, visible-light absorbing oxides such as Fe_2O_3 are more stable, but there is a smaller range over which the band energies can be controlled by size quantization. In a nanoscale composite system, denoted oxide-NP/TiO_2, the energy band alignments can inhibit interfacial electron transfer from the oxide-NP to TiO_2 as exemplified by the coupling of TiO_2 with Fe_2O_3 NPs in which the UV-light activity of TiO_2 declines, but without any visible-light response.[29, 30, 41]

Despite this, the change in electronic properties with the size of a metal oxide on going from the nano to molecular scale is an interesting scientific issue and the photocatalytic activity of an oxide-TiO_2 coupled system is interesting from the perspective of use as a catalyst. In this vein, Kisch and co-workers photosensitized TiO_2 using the impregnation method to graft metal halides such as the $PtCl_6{}^{2-}$ complex on TiO_2 [42].
This is an interesting approach because a visible-light response is induced by a simple synthesis approach and without introducing impurity or vacancy levels that promote recombination. Hashimoto and co-workers and Ohno and co-workers have presented a number of papers demonstrating an approach to grafting 3d metal ions including Cr^{3+},[43] Cu^{2+},[44] Fe^{3+} [45, 46] onto TiO_2. Grafting these 3d metal ions onto rutile TiO_2 can result in a high level of visible-light activity, but this effect is less significant for anatase; however, the surface modification idea is still quite attractive and is an alternative to the usual doping approach [46].
Our experimental collaborators in the group of Prof Tada developed a modification technique called chemisorption-calcination cycle (CCC), where a metal complex is adsorbed through strong chemical bonds and the organic ligand is then oxidized by post-heating, which allows for preparation of very small supported nanoclusters and ultrathin oxide films [47]. This experimental activity has worked together with our density functional theory (DFT) simulations, to provide a novel approach to modify TiO_2 for enhanced visible and UV photocatalytic activity for degradation of organic molecules. The present review summarizes our DFT studies metal oxide nanocluster modified TiO_2 (rutile and anatase), and the results are compared experiments. Section II describes the simulation methodology. Sections III is concerned with properties of MOs/TiO_2. Section IV presents new results on water-TiO_2 and the final Section provides a perspective on these new photocatalysts.

In our work using DFT simulations, we have successfully modified TiO_2 anatase and rutile surfaces with metal oxide nanoclusters (NCs) can be used to develop potential photocatalysts with some favourable properties. Namely

(1) modifying the light absorption properties of TiO_2, in many cases with predicted visible light absorption

(2) facilitate the spatial separation of photogenerated electrons and holes which will be useful in reducing charge recombination

(3) increase reactivity towards molecules such as CO by making it easier to form oxygen vacancies compared to unmodified TiO_2.

In this article we describe our previous results on a series of metal oxide nanocluster modified rutile and anatase systems, making comparisons with experiments from the group of Tada and co-workers, highlighting the effect of the oxide NCs on modifying the light absorption characteristics and electron-hole separation. Given that many experiments on photocatalysts are performed in aqueous solution or if water splitting is the application of interest, we need to go beyond simple ideal TiO_2 surfaces, which we term "dry" and consider the influence of water present on the TiO_2 surface, which we term "wet". Thus, we also present some new results on the stability of water on rutile and anatase at different surface coverages and how the wet surface can change the characteristics of NC modified TiO_2 compared to a dry surface by way of an explicit example. The study of water adsorption at TiO_2 surfaces has been presented in many studies and reviews [48–58]. Competition between molecular and dissociative adsorption of water is well studied for a single water molecule, while at higher coverages, mixed molecular/dissociated adsorption is usually observed.

The process of adsorption is, in general, determined by specific surface features like atomic coordination and surface defects, and in particular oxygen vacancies, which have been shown to play a fundamental role, not only in the adsorption process, but also in the reactivity of the surface with respect of specific reactions (e.g. potential site for CO_2 activation)[59, 60]. The presence and concentration of oxygen vacancies may depend on a number of factors, such as structural features, or the environmental conditions. While structural features only depend on the kind of crystal considered, environmental conditions depend on a number of physical-chemical parameters of the atmosphere and on the specific working condition of the process. Typically the oxygen in the atmosphere plays a fundamental role in the oxidation level of a given surface. However there is another crucial element which may play a crucial role. Water molecules present in the atmosphere may not only actively play a fundamental role in catalytic performance of CO_2 reduction, but also determine the oxidation level of the surface. However, the interplay of H_2O and surface oxygen vacancy under realistic environmental conditions is not completely clear. In view of this, a detailed analysis of water interaction with rutile (110) and anatase (101) TiO_2 surfaces, both stoichiometric and reduced, is crucial to determine their photo-catalytic properties.

We also investigate the interaction of water and oxygen vacancies, and the dependence of surface reduction on the water coverage on the surface . Although there have been a number of computational studies to analyse water adsorption on TiO_2 under vacuum conditions [48–58], in the present work we intend to examine the water-TiO_2 system in contact with two gas reservoirs, water vapour and oxygen, using *ab initio* atomistic thermodynamics, to reproduce realistic environmental conditions, as exemplified by our earlier work on CeO_2 [61, 62]. This analysis allows us to examine the effect of the composition of the atmosphere on water adsorption and oxygen vacancy formation energies. We will present a systematic DFT based analysis of H_2O adsorption on the stoichiometric and reduced rutile (110) and anatase (101) TiO_2 surfaces, using our DFT+U set-up described in Section II, with a Hubbard U correction on Ti 3d and O 2p electronic states (so that the photoexcited states can ultimately be consistently described for water covered surfaces). We compute water adsorption energies in vacuum and their dependence on the water coverage. Also, we analyse the effect of the water on the surface reduction.

,

II. REVIEW OF COMPUTATIONAL METHODS

In building models of metal oxide nanocluster modified TiO_2, we use a slab model of TiO_2 rutile (110) and anatase (101) and (001) surfaces, as shown in 1 1. A plane wave basis set is used to describe valence electronic wave functions using the VASP.5.2 code.[63]

The kinetic energy cut-off is 400 eV and to describe the core-valence interaction we apply Blöch's projector augmented wave (PAW) approach.[64] For Ti, we use 4 valence electrons throughout, having demonstrated in a number of papers that the important properties of interest for our work are not affected by using a 4 valance electron or 12 valence electron potential[65, 66] and for oxygen a 6 valence electron potential is used. In the oxide nanocluster modifiers we use the following valence electron potentials: for Ti, Sn, Pb, Ni, Cu and H - 4, 4, 4, 10, 11 and 1 valence electrons respectively. k-point sampling is performed using the Monkhorst-Pack scheme, with a (2×2×1) sampling grid. Throughout our work the Perdew-Wang 91 (PW91) approximation for the exchange-correlation functional is used.[67] Similar to studies of point defects in TiO_2 bulk and surfaces,[68–71] we use DFT corrected for on-site Coulomb interactions, the so-called DFT+U,[72] where U describes the Coloumb repulsion between electrons and is widely used in describing systems where localised electronic states are present; this includes well known systems such as oxygen vacancies in rutile (110), oxygen vacancies in CeO_2 and the ground state of transition metal monoxides. In these particular systems, the removal of a neutral oxygen vacancy will result in transfer of two electrons back to the oxide and these will reside on metal cations, thus reducing them, e.g. $Ti^{4+} + e^- \rightarrow Ti^{3+}$. The accepted understanding of this process is that the two electrons localise on two different metal sites in the oxide. Thus there are two reduced Ti^{3+} species in TiO_2 with one oxygen vacancy. There are well known difficulties with using standard approximate LDA and GGA functionals to attempt to describe this process and in the last decade, the DFT+U approach has proven rather popular and reasonably effective in describing metal oxides with such partially occupied electronic states, in particular for TiO_2. Since we have systems where partially occupied Ti_{3d} states are present, such as oxygen vacancy structures or photoexcited systems (described later), we apply DFT+U to the Ti_{3d} states, with a value of $U^{Ti_{3d}} = 4.5$ eV; for oxygen, to describe the hole in the valance band formed upon excitation, we apply $U^{O_{2p}} = 5.5.$ eV [73].

In our models, the rutile and anatase surfaces we have chosen are rutile (110) and anatase (001); for water adsorption we also examine anatase (101). Both surfaces are non-polar and the models are perfect surfaces, with no defects, such as oxygen vacancies, or hydroxyls, which can be present on real TiO_2 surfaces; work on such surface models is ongoing and some initial results are presented in Section IV of this review. Anatase (001) is accepted to be more active in photocatalysis than the most stable (101) surface and work in [74, 75] discusses how different schemes such as F-adsorption and Ag incorporation influences the stability of anatase (001).

For the rutile (110) surface, we use (4×2) and (4×4) expansions of the surface supercell to accommodate non-interacting nanoclusters of different sizes. For anatase (001) and (101), we use a (4×2) expansion of the surface supercell which is sufficient to isolate the adsorbed nanoclusters. The slab models are 6 O-Ti-O layers (18 atomic layers) thick for rutile (110), 6 O-Ti-O layers (18 atomic layers) thick for anatase (001), and 4 O-Ti-O layers (12 atomic layers) thick for anatase (101), with a 12 Å vacuum gap used throughout. All calculations are spin polarised with no restrictions on the overall spin. The convergence criteria for the energy and forces are 10^{-5} eV and 10^{-2} eV/Å^2, respectively.

The metal oxide nanocluster modifiers have been adsorbed on the TiO_2 surface in different configurations and relaxed with no constraints on the ionic positions of the dopant or the surface layers. For each configuration,

the adsorption energy of the metal oxide NC on rutile or anatase TiO_2 is calculated from:

$$E_{\mathrm{ads}} = E_{\mathrm{MO_x-TiO_2}} - [E_{\mathrm{MO_x}} + E_{\mathrm{TiO_2}}], \tag{1}$$

where MO_x is the metal oxide nanocluster and TiO_2 signifies rutile or anatase surfaces. Throughout this paper, a negative adsorption energy signifies that formation of an adsorbed NC on TiO_2 or water adsorption on TiO_2 are favoured.

We have extensively studied metal oxide nanoclusters with diameters less than 1 nm. This arises principally from the computational cost associated with the size of the nanocluster and the TiO_2 surface needed to accommodate the nanocluster: systems with between 300 and 900 atoms have been considered to allow TiO_2 nanoclusters up to 1.5 nm to be investigated. Larger oxide nanocluster modifiers (up to 3 nm) are being investigated but incurr significant computational expense.

We have also studied a simple model for the photoexcited state of a selection of nanocluster modified TiO_2 to examine two questions. The first is where the photoexcited electron and hole will be localised: in the surface, in the bulk, on the nanocluster and will localisation be favoured on any particular Ti or O species. Second, can the localisation and energies associated with electron and hole trapping be predicted from a simple ground state DOS analysis. To answer these questions, we have employed a model in which a triplet electronic state is imposed, as discussed in detail in refs. [73, 76–78] In this model an electron is "excited" to the CB with a corresponding hole in the VB by imposing a triplet electronic state. In determining the trapping (or relaxation) and the singlet-triplet excitation energies, we require the following calculations:

1. Single point energy evaluation of the triplet electronic state at the singlet geometry, giving $E_{\mathrm{unrelaxed}}$;

2. Full ionic relaxation of the triplet electronic state, E_{relaxed};

We add a dipole correction perpendicular to the surface plane to the total energies. Within this computational set-up, the following energies are calculated:

The singlet-triplet vertical (unrelaxed) excitation energy:

$$E_{\mathrm{vertical}} = E_{\mathrm{singlet}} - E_{\mathrm{unrelaxed}},$$

in which the singlet ground state is fully relaxed and the triplet state is fixed at the singlet geometry, corresponding to the VB-CB energy gap obtained from the PEDOS.

The singlet-triplet vertical excitation energy:

$$E_{\mathrm{excite}} = E_{\mathrm{singlet}} - E_{\mathrm{relaxed}},$$

where the singlet and triplet electronic states are fully relaxed. The change in this energy with respect to unmodified TiO_2 allows us to examine the effect of the surface modification on light absorption in TiO_2, which gives a crude approximation to the excitation energy.

The triplet relaxation (carrier trapping) energy:

$$E_{\mathrm{relax}} = E_{\mathrm{relaxed}} - E_{\mathrm{unrelaxed}},$$

where the first energy is the relaxed triplet electronic state and the second energy is the triplet electronic state fixed at the singlet geometry. E_{relax} is the energy gain after structural relaxation, when the electron and hole are trapped at their metal and oxygen sites. In considering these energies, the usual band gap underestimation is present arising using our DFT+U set-up, in which the values of U have been chosen to localise electrons and holes rather than reproduce the band gap of bulk TiO_2; the latter is a somewhat dubious approach. The relaxed singlet-triplet energy difference is smaller than the simple valence-conduction band energy gap, as it includes ionic relaxations and polaron formation in the response to "exciting" the electron. The vertical, unrelaxed singlet-triplet energy difference corresponds to the ground state VB-CB gap and this has also been discussed for rutile (110).[78]

This means that the key quantity is the comparison of the computed energies between different structures. We can state with confidence that a reduction in the singlet-triplet energy difference arising from surface modification of a metal oxide, relative to the unmodified metal oxide, will correspond to light absorption at lower energies in the modified oxide.

In Section IV, we will discuss the effect of water on oxygen vacancy formation and TiO_2 nanocluster adsorption. In this investigation, the surface energy, with adsorbed water, is calculated by taking into account the thermodynamic equilibrium of surface-adsorbate and the atmosphere.[62] The resulting surface energy is described as follows:

$$\gamma(p_i, \mathrm{T}) = \frac{1}{2A}\left[G - \sum_i N_i \mu_i(p_i, \mathrm{T})\right] \quad . \tag{2}$$

By using Eq.2 we can write the surface energy as a function of the chemical potential of the species in the atmosphere. In our case we consider an environment containing either only oxygen, or both water and oxygen.

The explicit account of pressure and temperature can be calculated from the expression of the chemical potential:

$$\mu_{\mathrm{i}}(p, \mathrm{T}) = \left[E_{\mathrm{i}} + \tilde{\mu}_{\mathrm{i}}(p^0, \mathrm{T}) + k_B \mathrm{T} \ln\left(\frac{p_{\mathrm{i}}}{p^0}\right)\right] \quad . \tag{3}$$

Here, the limit of the chemical potential are calculated to be:

$$\frac{1}{2}\Delta H_f(p = 0, \mathrm{T} = 0\mathrm{K}) < \Delta\mu_{\mathrm{i}}(p, \mathrm{T}) < 0 \quad , \tag{4}$$

where $\Delta H_f(p = 0, \mathrm{T} = 0\mathrm{K})$ is the heat of formation of TiO_2 and $\Delta\mu_{\mathrm{i}}(p, \mathrm{T}) = \mu_{\mathrm{i}}(p, \mathrm{T}) - \frac{1}{2}E_{\mathrm{O_2}}$. A detailed and explicit analysis of the equations can be found elsewhere.[62, 79, 80]

III. REVIEW OF DFT STUDIES OF METAL OXIDE NANOCLUSTER MODIFIED TIO_2

A. The modification of rutile (110) with TiO_2 Nanoclusters

We begin by describing our work on our model system of TiO_2 NC modified rutile (110) for which full discussions are presented in refs. [73, 77, 81].

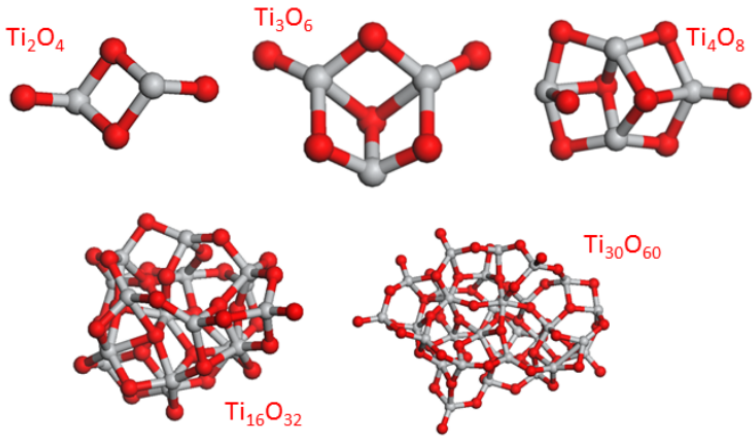

Figure 1: (Color online) Atomic structure of free TiO_2 nanoclusters. In this and all subsequent figures, Ti atoms are represented by grey spheres and oxygen atoms by red spheres.

Figure 1 shows the atomic structure of a series of TiO_2 nanoclusters that we have studied. We note here that the interesting features of the NCs are (1) there are low coordinated Ti and O sites in these nanoclusters; in particular we note singly coordinated terminal titanyl oxygen species and 3 and 4-fold coordinated Ti not found in bulk TiO_2. (2) At this length scale the atomic structure depends on the composition of the nanocluster. (3) The electronic properties, e.g. the valence band (VB) to conduction band (CB) energy gaps depend on the composition of the nanocluster.[82, 83] These features of TiO_2 NCs need to be kept in mind in discussing the effect of TiO_2 NC modification of TiO_2 surfaces.

Figure 2 shows the atomic structure of a selection of TiO_2 NC modified rutile (110) structures along with the computed adsorption energies referenced to a gas phase nanocluster and modified rutile (110) surface. The adsorption of the NCs at rutile (11) is favourable in all cases, as indicated by the large, negative adsorption energies, with the magnitude of the adsorption energy depending on the exact composition of the nanocluster. We also find that in contrast to gas phase TiO_2 nanoclusters, it is thermodynamically less favourable for these clusters to aggregate so that they are expected to remain adsorbed as discrete nanocluste rs rather than forming larger particles. The origin of this is most likely they strong binding of each nanocluster to the rutile (110) surface. Adsorption is accompanied by the formation of new Ti-O bonds between the nanocluster and the rutile (110) surface − these bonds are formed between 5-fold coordinated surface Ti atoms and oxygen in the nanocluster and between initially low coordinated Ti atoms in the nanocluster and bridging oxygen atoms on the rutile (110) surface. When we examine different adsorption modes of a given nanocluster composition at the rutile (110) surface there is a correlation between the magnitude of the adsorption energy and the number of new Ti-O bonds formed − with an increase in the latter, the adsorption of the NCs becomes stronger. While the detailed description of the atomic geometries are given in refs. [77, 81]

here we point out the following:

- that the new Ti-O bonds formed at the interface of the surface and the nanoclusters show similar Ti-O distances to bulk TiO_2

- the originally 5-fold coordinated Ti atoms in the surface that bind to oxygen from the NCs are pulled out of the surface layer

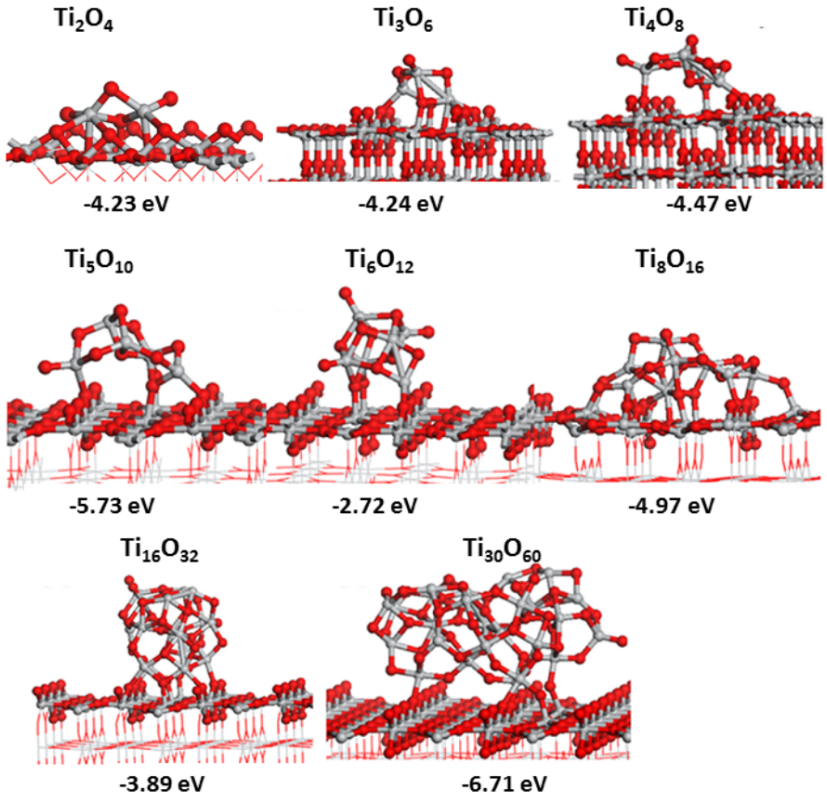

Figure 2: (Color online) Atomic structure of TiO_2 NC modified rutile (110). The composition (Ti_xO_{2x}) is given above each structure and shown under each structure are the computed adsorption energies in eV. Reproduced from reference [81], 2011 by permission of the PCCP Owner Societies and from ref. [77], 2013 Reproduced with permission from the Royal Society of Chemistry

- with the exception of the Ti_8O_{16} NC, all adsorbed nanoclusters keep at least one terminal, that is singly coordinated, titanyl oxygen species, which has very short Ti-O distances of $1.66 - 1.69$ Å

In our work on metal oxide NC surface modified TiO_2 a key result is the effect of the NC modification on light absorption of TiO_2 and whether the energy required to promote an electron from an occupied to an empty state, which will induce a red or blue shift in the absorption edge, is changed by the NC modification. We will discuss this point in terms of the potential shift in the absorption edge that would be measured by the UV-vis experiment, that is whether or not there will be a red shift towards the visible after surface modification. Given the inherent band gap underestimation with the DFT+U set-up used in our work what is important is whether there is a predicted red shift in the absorption edge and we will focus our discussion on this point throughout. Figure 3 shows the electronic density of states projected onto Ti_{3d} and O_{2p} states (PEDOS) for the TiO_2 NC modified rutile (110) surface for a selection of TiO_2 NCs. The PEDOS is shown for NC derived Ti and O species and surface derived Ti and O species. The first observation is that the surface VB to CB gap is unchanged from the bare (110) surface upon modification with the nanoclusters. The second observation is that after modification with these nanoclusters, there are new states present above the valence band edge of the rutile (110) surface and these originate from the TiO_2 nanoclusters. These new states push the valence band edge of the composite NC-surface system to higher energy and therefore will lead to a red shift in the absorption edge compared to the unmodified rutile (110) surface. The magnitude of the shift depends on the composition of the TiO_2 nanocluster. For example the Ti_3O_6 NC shifts the VB edge of the composite structure by 1.3 eV over unmodified rutile (110), while the $Ti_{16}O_{32}$ modification induces a smaller shift of 0.4 eV. In all composite

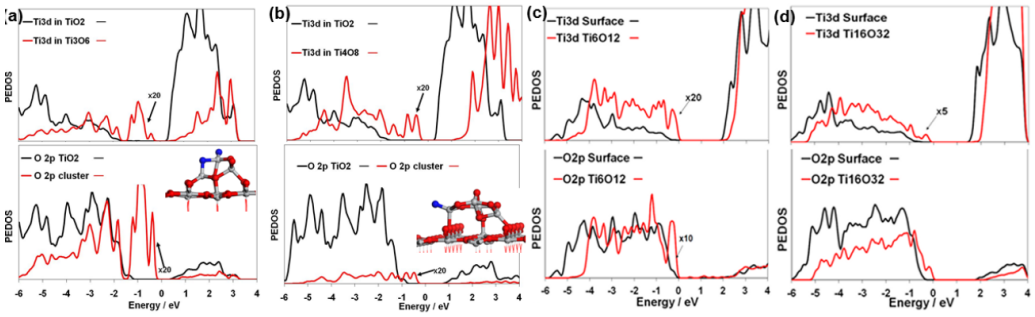

Figure 3: (Color online) Projected density of sates for TiO_2 NC modified rutile TiO_2 (110). Reproduced from reference [81], 2011 by permission of the PCCP Owner Societies and from ref. [77], 2013 Reproduced with permission from the Royal Society of Chemistry

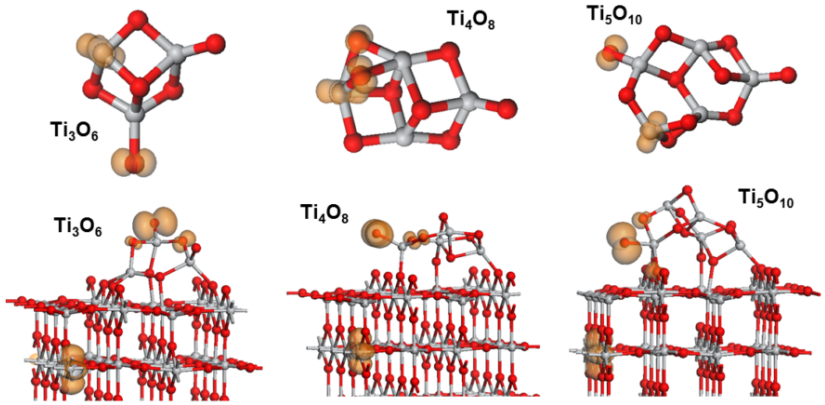

Figure 4: (Color online) Spin density plots for a selection of free TiO_2 nanoclusters Ti_3O_6, Ti_4O_8 and Ti_5O_{10} (top panel) and for the same TiO_2 nanoclusters supported on rutile (110) (bottom panel). The spin density isosurfaces enclose spin densities of 0.02 eV/$\AA^3$. Reproduced from ref. [73], 2014, with permission from the American Chemical Society

structures, the bottom of the conduction band is derived from empty Ti_{3d} states from the rutile (110) surface. For the examples of Ti_3O_6 and Ti_4O_8 nanoclusters, we also show in Fig. 3 the oxygen atoms of the nanocluster that contribute most significantly to the new nanocluster derived O_{2p} states that push the VB edge to higher energy. It is important to note that these oxygen atoms are those with the lowest coordination in the respective TiO_2 nanoclusters and we will return to this point in later sections of this review. A final observation which is the second crucial factor for the photocatalytic properties of these structures concerns the fate of photoexcited electrons and holes. As described in detail in refs. [73, 84, 85], we have used a simple model to examine the nature of the photoexcited state. This is constructed by imposing a triplet electronic state on the system which means that an electron is now in the previously empty conduction band and there is a hole in the valence band and we can therefore investigate the nature of the photoexcited state in these structures.

Figure 4 shows the spin density plots (spin density plots show where the two unpaired electrons are located) for a selection of free TiO_2 nanoclusters (top panel) and for the same TiO_2 nanoclusters supported on rutile (110) (bottom panel). For the free nanoclusters the hole localises on a low coordinated oxygen atom, e.g. for Ti_3O_6 and Ti_5O_{10} (as well as other larger nanoclusters, see ref. [73]) the hole is found on the singly coordinated titanyl oxygen. For Ti_4O_8, the hole spreads over two two-coordinated oxygen atoms; interestingly, this was also found using TDDFT simulations in the work of Berardo *et al.*.[86]

The electron is localised onto a low coordinated Ti atom in all cases – for these NCs the Ti atom is 3 coordinated. As discussed in ref. [73], Bader charges and spin magnetisation confirm localisation of a hole (with

an O_{2p^5} configuration) and an electron (giving reduced Ti^{3+} on the oxygen and Ti atoms just described. In addition, the resulting Ti^{3+}-O^{2-} and Ti^{4+}-O^{-} distances are elongated which is well known for such polaronic states. When these NCs are supported on the rutile (110) surface the hole and electron are now localised onto the TiO_2 nanocluster and the rutile (110) surface, respectively. This spatial separation of hole and electron upon excitation is predicted from the analysis of the character of the valence band and conduction band PEDOS in the ground state. Similar to the free nanoclusters, the hole localises onto a titanyl oxygen where one is available. This highlights the key role of low coordinated oxygen sites in hole localisation. The hole and electron separation has the potential consequence that upon excitation charge recombination will be reduced over the unmodified rutile (110) surface which can enhance photocatalytic activity.

B. The modification of rutile (110) and anatase (001) with Transition Metal Oxide Nanoclusters

In a number of papers with the group of Tada[87–90], we have studied the modification of rutile and anatase TiO_2 surfaces with nanoclusters of transition metal oxides. These include NiO[87] and CuO[90], while we also published an early DFT study of FeO_x modified rutile (110), [91]. The choice of these FeO_x is motivated initially by the work from Tada *et al.*[40][92] and Libera *et al.*[93] who fabricated FeO_x-modified TiO_2 materials and found visible light absorption and enhanced photocatalytic activity compared to unmodified TiO_2. The choice of other modifiers comes from our colalboration with Tada. In this section we describe our simulation results on these systems, making comparisons to experimental work where available.

Figure 5 shows the relaxed atomic structure and computed adsorption energies (referenced to free FeO_x and bare rutile (110) surface) for the Fe_2O_2 and Fe_2O_3 nanocluster modification of rutile (110). Negative adsorption energies in figure 5 show that iron oxide nanoclusters are stable upon adsorption at the rutile (110) surface. The magnitude of the adsorption energy indicates that these adsorbed nanoclusters should be thermally stable. In the most stable adsorption structure of Fe_2O_3, the O and Fe atoms from iron oxide are arranged in a zig-zag pattern: O-Fe-O-Fe-O. Such a structure is also typical of the structure of the most stable gas phase Fe_2O_3 cluster. Each O interacts with a 5-fold coordinated Ti atom lying along a row in the rutile (110) surface; this binding site is known for oxygen adsorbed on the rutile (110) surface. In adsorbed Fe_2O_3 the Fe-O distances are 1.82 Å and 1.93 Å; the two Fe cations bind with the second oxygen . The Fe-O distances to TiO_2 oxygen lie in the range $2.02 - 2.09$ Å and the Ti-O distances involving oxygen from the Fe_2O_3 nanocluster lie in the range $2.1 - 2.2$ Å.

In $(FeO)_2$, the Fe cations are bound to two bridging oxygen on rutile (110); the Fe-O distances are 2.11, 2.29 Å. Oxygen from the $(FeO)_2$ nanocluster binds to a 5-fold coordinated surface Ti atom , with a Ti-O distance of 1.89 Å. The Fe-O distances in the iron oxide cluster are 2.04 and 2.12 Å.

The PEDOS plots of FeO_x adsorbed at TiO_2 shown in Fig. 5 show that adsorption of the nanocluster results in the formation of new electronic states, derived from the adsorbed FeO_x nanoclusters. These new states lie above the original rutile (110) valence band edge. Therefore, iron oxide adsorption at the rutile (110) surface has pushed the top of the valence band upwards in energy. The bottom of the conduction band is dominated by the empty Ti_{3d} states originating from surface Ti atoms. The consequence of the interaction between iron-oxide nanoclusters and TiO_2 is that as a result of the shift of the valence band to higher energy, the band gap of the composite structure will be narrowed by comparison with unmodified TiO_2 and there is a red shift in light absorption; we predict a shift of around 0.3 eV that suggests visible light absorption will be possible.

Finally, the positions of the FeO_x and rutile (110) electronic states is proposed to facilitate charge separation

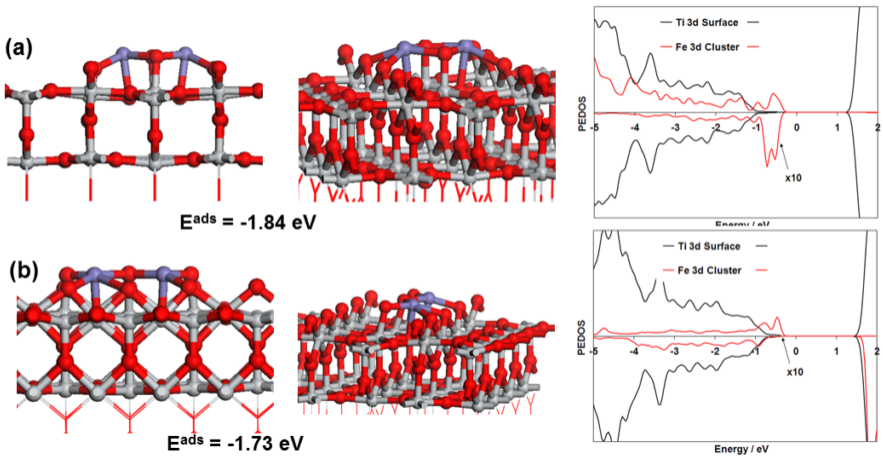

Figure 5: (Color online) (a): Atomic structure, computed adsorption energy and Ti_{3d}/Fe_{3d} PEDOS for rutile TiO_2 (110) modified with an $(FeO)_2$ nanocluster. (b) Atomic structure, computed adsorption energy and Ti_{3d}/Fe_{3d} PEDOS for rutile TiO_2 (110) modified with an Fe_2O_3 nanocluster. Reproduced from reference [91], 2011 by permission of the PCCP Owner Societies

after excitation. Upon absorption of visible light, excited electrons will be found on the TiO_2 support and the valence band holes will be found on the iron oxide nanocluster. Thus, electrons and holes will be naturally spatially separated and this will reduce the possibility of electron-hole recombination.

Together with the group of Tada *et al.* we presented two combined modelling and experimental studies of NiO-modified TiO_2 and CuO-modified TiO_2.[87, 90]

The atomic structure and PEDOS for examples of Ni_4O_4-nanocluster modified anatase (001) and rutile (110) are shown in Fig. 6 (a) and (b). Both NiO nanoclusters adsorb at the TiO_2 surfaces with strong gains in energy again indicating formation of new surface-nanocluster bonds. When anatase is modified with the Ni_4O_4 nanocluster there are six new bonds formed and a surface oxygen atom is pulled out of the surface by 0.19 Å. In the Ni-O nanoclusters Ni-O distances are shorter when compared to Ni-O distances in bulk NiO, e.g. 1.95 Å in Ni_4O_4, compared to 2.10 Å in bulk NiO. On rutile (110), adsorption of the Ni_4O_4 nanocluster results in formation of eight new bonds; three of the Ni atoms create four new Ni-O bonds to bridging surface O atoms. The shortest Ni-O distance is 1.96 Å and the longest Ni-O distance is 2.22 Å. Two bonds are from oxygen in the nanocluster binding with Ti in the surface. In these structures, any surface Ti atoms that bind to oxygen from the nanocluster are pulled out of the surface plane, with displacements of $\sim$ 0.5 Å.

Fig. 6 shows the PEDOS for Ni_{3d} and Ti_{3d} states for the examples of the Ni_4O_4 nanocluster rutile and anatase surfaces. The PEDOS shows that by modifying TiO_2 with NiO, new electronic states derived from the NiO nanocluster are introduction and these lie above the top of the valence band edge of the anatase and rutile surfaces. This shifts the valence band edge of nanocluster-modified TiO_2 system to higher energy when compared to the unmodified surfaces. The bottom of the conduction band of the NiO-modified surfaces is dominated by surface Ti_{3d} states. In ref. [87], we showed that a closer examination of the conduction band states for some NiO-modified anatase structures indicates that there are structures, e.g. Ni_2O_2, in which empty NiO cluster levels are present at the conduction band minimum. Thus, the nature of the valence and conduction band edges can depend on the composition of the NiO nanocluster modifier.

Fig. 7 shows the atomic structure and PEDOS for anatase (001) and rutile (110) modified with CuO nanoclusters with different compositions, namely CuO and Cu_4O_4. On the TiO_2, surfaces the computed adsorption energies indicate a strong adsorption of CuO nanoclusters and this is driven by formation of

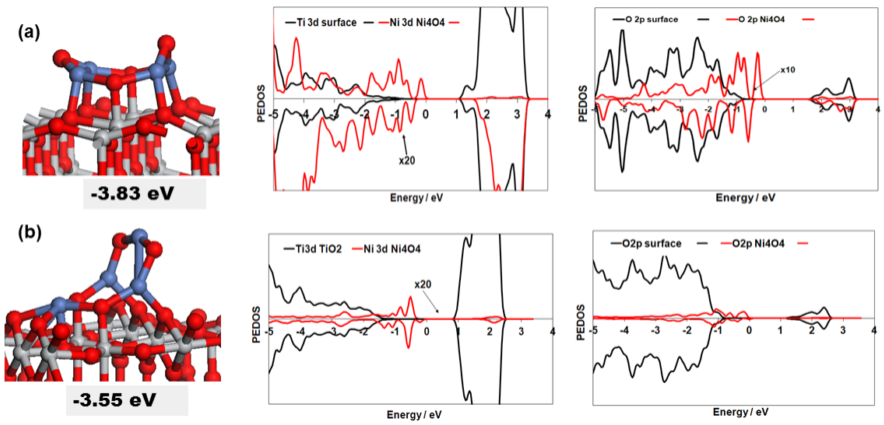

Figure 6: (Color online) (a): Atomic structure, computed adsorption energy and Ti_{3d}/Ni_{3d} and O_{2p} PEDOS for anatase TiO_2 (001) modified with an $(NiO)_2$ nanocluster. (b) Atomic structure, computed adsorption energy and Ti_{3d}/Fe_{3d} and O_{2p} PEDOS for rutile TiO_2 (110) modified with an $(NiO)_4$ nanocluster. Reproduced from ref. [87], 2013, with permission from the American Chemical Society

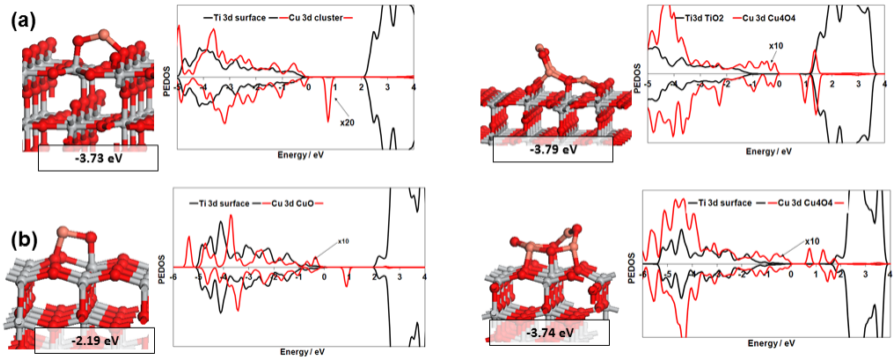

Figure 7: (Color online) (a): Atomic structure, computed adsorption energy and Ti_{3d}/Cu_{3d} and O_{2p} PEDOS for rutile TiO_2 (110) modified with CuO and $(CuO)_4$ nanoclusters. (b) Atomic structure, computed adsorption energy and Ti_{3d}/Cu_{3d} and O_{2p} PEDOS for anatase TiO_2 (001) modified with CuO and $(CuO)_4$ nanoclusters. Reproduced from ref. [90], 2013, with permission from the American Chemical Society

interfacial Cu-O and Ti-O bonds between the nanoclusters and the surface.

On Rutile (110), the smallest CuO nanocluster has a Cu-O distance of 1.79 Å to bridging surface oxygen and a Cu-O distance of 1.76 Å in the nanocluster. A 5-fold coordinated surface Ti binds to oxygen in the nanocluster, with a distance of 1.87 Å. The adsorbed $(CuO)_4$ nanocluster displays bonding between three Cu atoms in the nanocluster and 2-fold bridging oxygen atoms in the surface. The resulting Cu-O distances to the surface are 1.95, 1.96 and 2.1 Å. 5-fold coordinated surface Ti atoms bind to two oxygen atoms of the nanocluster, giving Ti-O distances of 1.91 Å. In the adsorbed nanocluster Cu-O distances lie in the range of 1.73 to 1.95 Å.

On anatase (001), the CuO nanocluster adsorbed with the Cu atom coordinated to a 2-fold coordinated oxygen in the surface and the Cu-O distance is 1.91 Å. Oxygen in the CuO nanocluster binds to a 5-fold coordinated surface Ti, with a Ti-O distance of 1.80 Å. This particular oxygen and a surface Ti atom are displaced away from the surface layer by 0.17 and 0.34 Å, respectively, upon interaction with CuO. The Cu-O distance in the nanocluster is 1.76 Å.

Upon adsorption of the $(CuO)_4$ nanocluster, three nanocluster Cu atoms form new Cu-O bonds to the 2-coordinated surface oxygen. The Cu-O distances are 1.88, 1.91 and 1.91 Å. These surface oxygen are

displaced upwards out of the surface plan. Two nanocluster oxygen atoms bind to Ti atoms on the surface, with Ti-O distances of 1.94 and 2.03 Å. The Cu-O distances in the nanocluster can be divided into two groups. In the first group, that involves low coordinated oxygen that do not bind to atoms in the surface, the Cu-O distances are in the range $1.76 - 1.78$ Å. The second group, is those oxygen binding to Ti in the surface and the Cu-O distances are $1.86 - 1.89$ Å.

Fig. 7 also shows the PEDOS for CuO and $(CuO)_4$ nanoclusters adsorbed on the anatase and rutile surfaces. The PEDOS show that CuO nanocluster modification of anatase and rutile surfaces can cause a significant change in the TiO_2 energy bands at both the valence and conduction band edges. Furthermore the VB and CB modification strongly dependent on the size of the CuO nanocluster, as discussed in ref. [90].

For modification of anatase and rutile with a CuO nanocluster (n = 1) there are new, unoccupied Cu_{3d} states in the VB-CB gap and these are consistent with the presence of a Cu^{2+} oxidation state. If we now consider the impact of the CuO-loading (CuO nanocluster size) on rutile (110), there is some interesting behavior: namely, with increasing CuO nanocluster size, there is a significant upwards shift in the top of VB, which is ~ 0.7 eV for Cu_4O_4-modified rutile (110). The origin of this is the CuO derived occupied states that are found at higher energy than the surface VB edge. At the same time, the empty Cu^{2+} states, previously in the energy gap, are shifted upwards in energy to approach the TiO_2 CB minimum.
While an increase in CuO loading (size) induces a narrowing of the band gap compared to unmodified TiO_2, the precise origin of the band gap narrowing depends on the CuO loading. Given this CuO loading dependence in the origin of the band gap change in CuO-modified, this provides an interesting possibility that control of CuO loading is a useful tool to tune the mechanism of the band gap reduction and, additionally, the nature of the photoexcitation, which will determine the activity of the photogenerated electrons and holes.

We now discuss the results from experimental studies of FeO_x, NiO- and CuO-modified TiO_2. We briefly recall that in the work of Tada *et al.*, the metal oxide nanocluster modifiers are loaded onto the TiO_2 through the CCC approach in which an organometallic precursor of the target metal is adsorbed onto TiO_2 and the system is calcined, which removes the organic ligand and oxidises the metal. Repeated application of this cycle increases the loading of the metal oxide modifier. Fig. 8 shows some key results from experimental work [40, 87, 89, 90], namely the UV-vis absorption spectrum and valence band edge XPS spectrum of NiO-modified TiO_2 (Figs. 8 (a), (b) and (c)) and the UV-vis and valence band edge XPS spectrum of CuO-modified TiO_2 (Figs. 8 (d), (e) and (f)).
For FeO_x-modified TiO_2, Jin *et al.* [92] showed a red shift in the absorption edge to longer wavelength. Valence Band Photoemission Spectroscopy was used to show that the top of the VB moves to higher energies upon modification of TiO_2 with the FeO_x nanoclusters. This is consistent with our DFT results that show, irrespective of the Fe oxidation states (2+ or 3+), an upwards shift of the valence band edge when TiO_2 is modified with iron oxide nanoclusters. It is also important to note that the experiments show a clear shift of the VB edge to higher energy and not the appearance of a new dopant-induced electronic state in the TiO_2 VB to CB energy gap; the latter is the usual situation with respect to substitutional doping in TiO_2
For NiO-modified TiO_2 the experimental work shows a red shift in the absorption edge with NiO loading on TiO_2. The VB photoemission spectrum shows a clear upwards shift of the valance band edge with increased NiO loading. Again, these results are consistent with the results of from DFT level simulations that indicate the VB edge moves to higher energy with NiO modification. The rise in the VB edge is large enough to induce

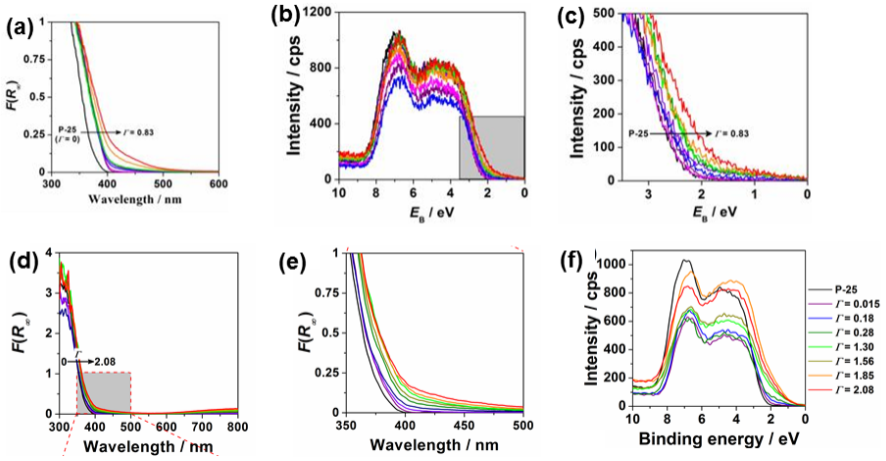

Figure 8: (Color online) (a) UV-vis absorption spectrum, (b) Valence band XPS spectrum, with a zoom into the shaded region shown in part (c) for NiO nanocluster modified TiO_2. (d) UV-vis absorption spectrum, with a zoom into the shaded region shown in part (e) and (f) Valence band XPS spectrum for CuO nanocluster modified TiO_2. Reproduced from refs. [87, 90], 2013, with permission from the American Chemical Society

a red shift in the absorption edge, but at higher loadings the shift is so large that the oxidative power of the holes is reduced and the photocatalytic activity of NiO-modified TiO_2 shows a maximum as a function of NiO loading. In fact, this is a phenomenon that has been observed in experimental work.

For CuO-modified TiO_2, upon increasing the CuO loading on TiO_2, there is a significant red shift in the absorption edge to longer wavelength, thus inducing visible light absorption. An interesting point is the effect of the CuO loading on the electronic structure and the origin of the red shift. The valence band photoelectron spectroscopy results in 8 (d) suggest that there are two distinct regimes that depend on the CuO loading. At the lowest CuO loadings, there is a small upshift of the valence band edge. There is then a significant increase in the upshift of the VB edge at loadings larger than 1.30 Cu / nm^2. The red shift in the absorption edge appears to increase with CuO loading, with a different dependence. Our simulation results suggest that for low CuO coverages the empty Cu 3d states characteristic of Cu $^{2+}$ lie below the energy of the conduction band, with an insignificant upshift of the valence band edge; thus the excitation is from the TiO_2 VB to the empty Cu 3d states. When the CuO coverage increases, the CuO electronic states move to higher energy so that the VB edge is shifted to higher energy by virtue of the presence of CuO derived srates and the empty in-gap Cu 3d states shift to energies above the TiO_2 conduction band edge. This can be seen in the strong upwards shift of the valence band edge from the VB photoelectron spectroscopy results at higher CuO loadings.

Identifying the presence of the metal oxide nanocluster modifier on TiO_2 is very challenging as techniques such as TEM or X-Ray diffraction will not allow the modifier to be characterised. To date, the effect of the oxide modifier on the key properties for photocatalysis have been examined and these are used to characterise the successful modification of TiO_2. It is important to remember that for many surface modified TiO_2 systems, experimental results [32, 35, 40, 92] show that in the composite system, there is a clear shift of the valence band edge to higher energy relative to unmodified TiO_2. Also, some studies have compared modified TiO_2 to the bulk metal oxide modifier, e.g. SnO_2 [89] and PbO [94], which is discussed below. In these cases, it is demonstrated that bulk phases of the metal oxide modifier are not present.

If we compare to doping, in which new dopant-induced electronic states are formed in the TiO_2 band gap rather than shifting the valence (or conduction) band edge, then we can see a clear difference between the two modifications of TiO_2: doping results in formation of localised electronic states that can enhance recombination,

but surface modification avoids this potentially fatal problem. In fact photluminesence data for modified TiO_2, e.g. ref. [40] shows that the typical TiO_2 photoluminesence feature is quenched when the surface modification scheme is used.

C. Effect of Metal Oxidation State: SnO/SnO_2 and PbO/PbO_2 Nanocluster Modified Anatase (001)

Another interesting phenomenon in the choice of metal oxide modifier is the ability to tune the resulting red shift and the nature of the photoexcited state by the choice of the oxidation state of the metal oxide nanocluster modifier. We have investigated in detail two examples and experimental data is now also available to support our findings. The oxides of interest here are (1) SnO/SnO_2 and (2) PbO/PbO_2. Both Sn and Pb have +2 and +4 oxidation states, with the +2 oxidation state having an electronic configuration: s^2p^2. The +2 oxidation state of both cations is key to the well known stereochemical lone pair in the bulk SnO and PbO systems which are characterised by a distorted atomic structure as described in a number of publications.[95–97]

To examine the effect of the Sn oxidation state on SnO_x-modified TiO_2 Fig. 9 shows the atomic structure and the PEDOS of Sn_2O_4 and Sn_2O_2 modified anatase (001), and we discuss the differences between the Sn oxidation states; results for other SnO_x nanoclusters are described in detail in refs. [77, 89].

The SnO_2 and Sn_2O_2 nanoclusters adsorb strongly at the anatase (001) surface with adsorption energies of -5.29 eV and -2.92 eV that indicate a strong interaction between the SnO_x nanoclusters and the anatase (001) surface. This is particularly clear when one sees that oxygen atoms in the anatase (001) surface are strongly displaced from their surface sites to interact with the SnO_x nanoclusters. For the Sn_2O_4 cluster, the displaced surface oxygen and oxygen from the nanocluster are found in similar bonding environments; the surface oxygen atoms are displaced by 1.11 Å. Sn-O distances are $2.10 - 2.15$ Å. The adsorption of the Sn_2O_2 nanocluster results in formation of new cluster-surface bonds; the distances between Sn in the nanocluster and oxygen in the surface are 2.11 and 2.15 Å in Sn_2O_2. For comparison the Sn-O distances in SnO litharge are 2.26 Å and the Sn-O distances in Sn_2TiO_4 are 2.09 and 2.21 Å so the smaller SnO cluster has Sn-O distances similar to litharge.

The most significant effect of the Sn oxidation state is seen in the changes to the electronic structure of anatase upon modification with the SnO_x nanoclusters, as shown in the PEDOS plots in Fig. 9. The SnO_2 nanocluster modification results in no significant changes to the valance or conduction band edges; there is a small Sn 5s contribution to the bottom of the conduction band and an O_{2p} contribution from SnO_2 oxygen atoms around 1 eV below the valence band edge. Thus, modification with SnO_2 should result in no shift in the absorption edge compared to unmodified anatase. There is a different effect arising from modification with SnO in which SnO-derived states are present above the valence band edge of anatase; for this particular nanocluster a small red shift of 0.3 eV would be expected which would push light absorption towards the visible region. The effect of the Sn^{2+} oxidation state is to induce states derived from the Sn_{5s}-O_{2p} interaction that are typical of this oxidation state of Sn and have been widely discussed in terms of the stereochemical lone pair in SnX (X = O, S, Se) solids.

For PbO, PbO_2 nanoclusters (Pb_2O_2, Pb_2O_4), the atomic structures of modified anatase are shown in Fig. 10.[85] The computed adsorption energies are -6.68 eV and -6.64 eV for Pb_2O_2 and Pb_2O_4 nanocluster adsorption, respectively. This again illustrates a strong interaction between the nanocluster and TiO_2. The key point for our discussion is the effect that the Pb oxidation state has on the electronic structure of PbO_x-modified

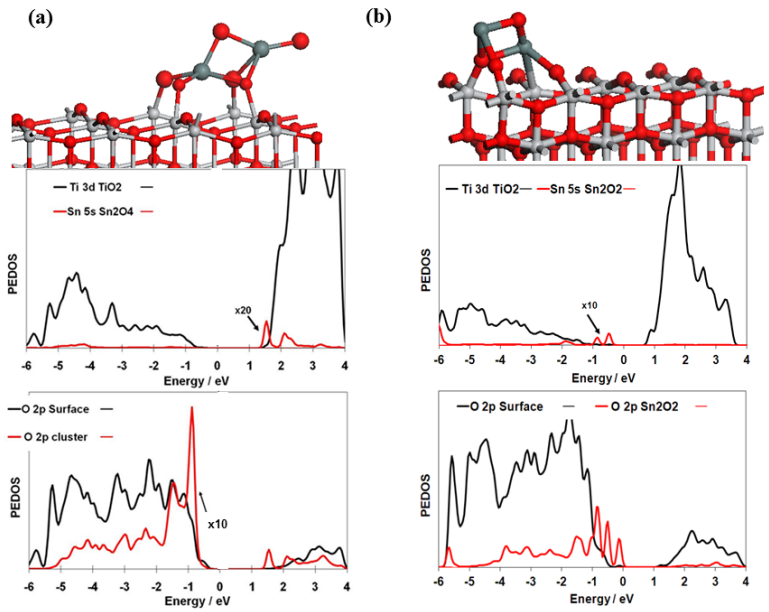

Figure 9: (Color online) (a): Atomic structure and Ti_{3d}/Sn_{rm5s} and O_{2p} PEDOS for SnO_2 modified anatase (001). (b): Atomic structure and Ti_{3d}/Sn_{rm5s} and O_{2p} PEDOS for SnO modified anatase (001). Reproduced from ref. [89], 2013, with permission from the American Chemical Society and ref. [98], 2012, with permission from the Royal Society of Chemistry

anatase its role in determining the nature of the photocatalytic properties. For PbO-modified anatase, there are new PbO derived Pb 6s and O_{2p} states found lying above the anatase valence band edge . The presence of these states will shift light absorption to longer wavelength, potentially into the visible region. By contrast when the PbO_2 nanocluster is adsorbed at anatase (001) there are empty Pb 6s states lying below the empty Ti3d conduction band states of anatase. This will also result in a red shift in light absorption but the mechanism in the red shift will depend on the oxidation state of Pb.

The final aspect of these modified TiO_2 structures to consider is the nature of the photoexcited state and for this Fig. 11 shows the spin density plot for the relaxed triplet excited state for the example of SnO-anatase (001). This plot shows that the electron resides on a Ti atom from anatase and the hole resides on Sn-O moieties in the SnO nanocluster. The electron and hole localisation are consistent with the composition of the valence and conduction band edges of the SnO-anatase system.

While the DFT results described above give clear predictions of the effect of SnO_x and PbO_x nanocluster modification of anatase TiO_2, these need to be confronted by experiment. Therefore, in Fig. 12 we show experimental results for SnO_2-modified TiO_2 (Fig. 12 (a)), SnO-modified TiO_2 (Fig. 12 (b)) and PbO-modified anatase TiO_2 (Fig. 12 (c).

Figure 12 (a) shows that there is no change in the absorption edge of anatase TiO_2 when modified with SnO_2; while one SnO_2 loading is shown, this result is found for all loadings considered. The second important result is that the VB edge from VB XPS spectroscopy is hardly changed after modification with SnO_2 [88]. Comparison of the photoelectron spectrum of SnO and SnO_2 shows that these phases are not present. There is therefore, no shift in the absorption edge when using SnO_2 as the modifier of anatase, consistent with our DFT results. While there is no visible light activity in this composite system there is some enhancement of UV activity.

Figure 12 (b)shows experimental results for the UV-vis and the valence band photoelectron spectroscopy spectrum for SnO-modified TiO_2 from ref. [99]. SnO-modified TiO_2 is prepared by adding titanium tertbutoxide

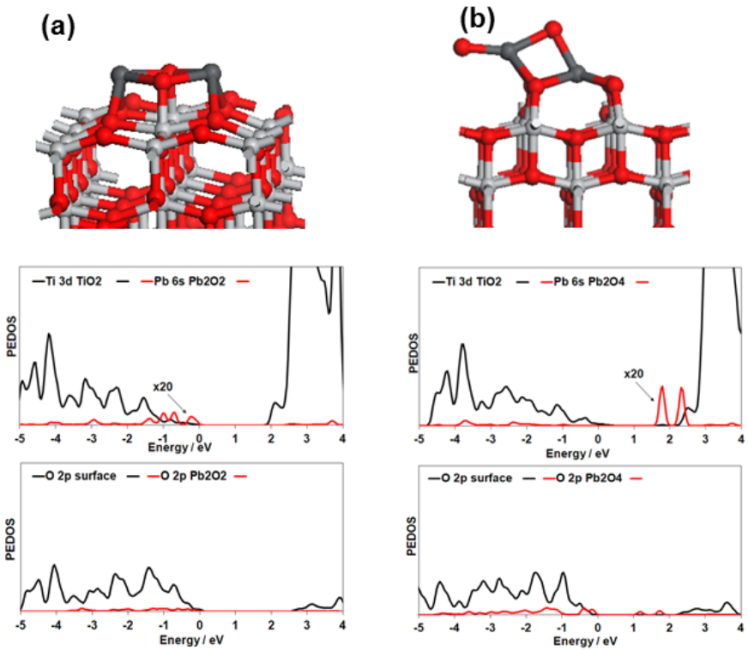

Figure 10: (Color online) (a): Atomic structure and Ti_{3d}/Pbm 6s and O_{2p} PEDOS for PbO modified anatase (001). (b): Atomic structure and Ti_{3d}/Pb 6s and O_{2p} PEDOS for PbO_2 modified anatase (001). Reproduced from ref. [85], 2013, with permission from the Royal Society of Chemistry

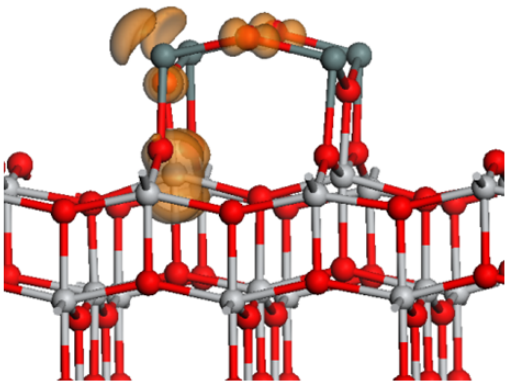

Figure 11: (Color online) Spin density plot (enclosing isosurfaces of 0.02 eV/Å) for the relaxed triplet electronic state of SnO modified anatase (001). The spin density plots show the location of the photoexcited electron and hole. Reproduced from ref. [84], 2013, with permission from the Royal Society of Chemistry

$(Ti(OBu)_4)$ to aqueous tin chloride in which the $Ti(OBu)_4$ is hydrolysed. The effect of the SnO modification of TiO_2 is to introduce a significant red shift in the absorption edge when compared with unmodified TiO_2 (which is indicated by "inf" in the spectrum of Fig. 12 (b)). From this work, the magnitude of the red shift can be 0.73 eV which is a significant change and will induce visible light absorption. This shift is also consistent with the large reduction in the energy gap predicted from our simulations. The VB photoelectron spectrum also shows that the valence band edge of the composite system is shifted to higher energy compared to unmodified TiO_2, which is the origin of the red shift in the absorption edge and is also consistent with the shift in the vlence band found from our simulation results.

Figure 12 (c) shows the UV-vis spectrum and the valence band photoelectron spectrum for PbO-modified TiO_2 from ref [94]. PbO-modified TiO_2 is prepared by using aerosol assisted CVD to deposit TiO_2 on glass and

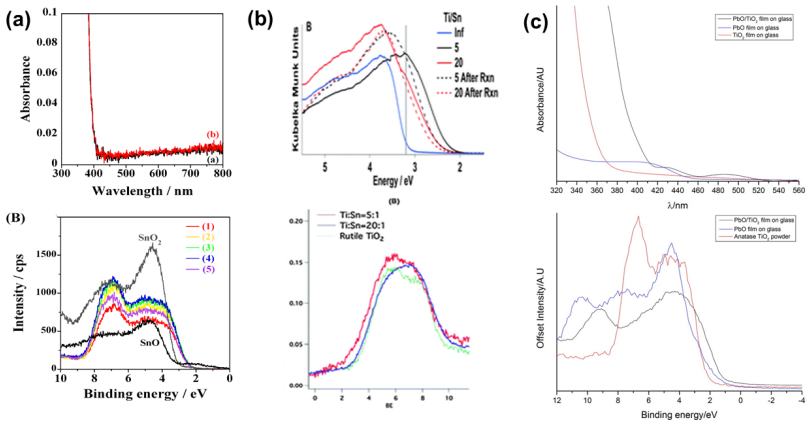

Figure 12: (Color online) (a): UV-vis and valence band XPS spectra for SnO_2-modified anatase TiO_2, (b):UV-vis and valence band XPS spectra for SnO-modified TiO_2 (c): UV-vis and valence band XPS spectra for PbO-modified anatase TiO_2. Reproduced from ref. [89], 2013, and ref. [94], 2014, with permission from the American Chemical Society. Reproduced from ref. [99], 2013, by permission of the PCCP owner societies

then deposit litharge structured PbO on TiO_2. The UV-vis spectrum shows that modification of anatase with PbO results in a significant red shift of the absorption edge to longer wavelength. Comparison with unmodified TiO_2 and pure PbO films shows that the PbO modification clearly changes the light absorption characteristics of TiO_2. The valence band photoelectron spectrum shows that the VB edge of PbO-TiO_2 shifts to higher energy after PbO modification and a significant shift of 1 eV in the valence band edge is found so the impact of PbO modification is rather strong. This work also showed that no PbO_2 phases are present, which is important to show the stability of the PbO-modified TiO_2 composite system.

In a final example of modifying a non-TiO_2 material, Boppana *et al.*[100] also examined $ZnGa_2O_4$ modified with SnO and SnO_2 and found that any visible light absorption (or a shift from unmodified $ZnGa_2O_4$) was entirely due to the presence of SnO, with no shift found when only SnO_2 was used.

When comparing the DFT simulations to the, so far limited, experimental work, it is clear that there is a good correspondence between the findings of DFT simulations of these p-block metal oxide nanocluster modified systems and the available experimental results. A particularly interesting insight is that the oxidation state of Sn or Pb can be used to control both the appearance of a shift in the absorption edge and the mechanism underlying this shift.

IV. ADSORPTION OF WATER AT RUTILE AND ANATASE TIO_2 SURFACES

A. Water on stoichiometric and reduced rutile(110) and anatase (101)

1. Geometries

Firstly, we consider the adsorption of water molecules on the rutile (110) and anatase (101) stoichiometric surfaces. In a (2×2) surface expansion, eight titanium sites are available on the surface layer of both surfaces for water adsorption. When a single H_2O molecule is adsorbed on the surfaces, resulting in a 1/8 monolayer (ML) coverage, we found non dissociative molecular adsorption on both anatase (101) and rutile (110) surfaces, which is consistent with the literature [56] After geometry relaxation the Ti-O distance is 2.18 Å in rutile and

2.12 Å for anatase. When the coverage increases to 3/8 we found a different trend for the two cases, and, while a non dissociative adsorption is found on rutile, partial water dissociation takes place on anatase. For 3/8 ML coverage the Ti-O distances are 2.15, 2.18, 2,23 Å in rutile (110), while for anatase (101) the same bond distance measured to be 2.15 and 2.16 Å. When six water molecule have been adsorbed on the same surface (6/8ML), then, a spontaneous dissociative adsorption takes place on both surfaces, and bond-lengths of 1.97 Å and 0.97 Å has been obtained for Ti-O and H-O bonds, respectively, in rutile (110), while the same values are 1.90 Åand 0.97 Å in anatase (101). An illustration of the dissociative and non dissociative adsorption at different coverages on rutile and anatase surface is shown in Figs. 13 and 14. The O-H distances obtained here after hydroxylation are comparable with other works in literature.[62]

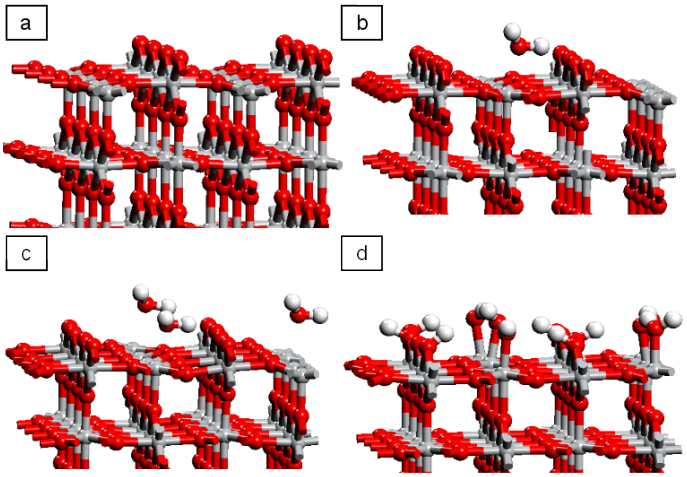

Figure 13: (Color online) Atomic structure of rutile TiO_2(110) stoichiometric surface under (a) dry conditions and with water adsorbed at (b) 1/8, (c) 3/8 and (d) 6/8 ML coverages. Gray, red and white spheres represent titanium, oxygen and hydrogen, respectively

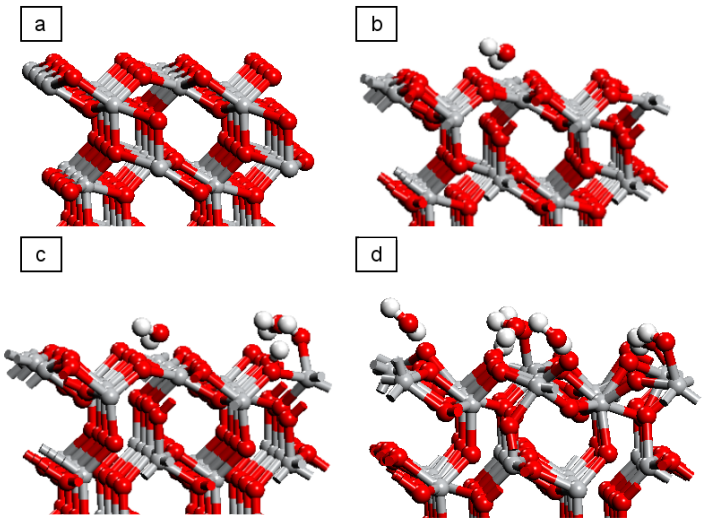

Figure 14: (Color online) Atomic structure of anatase TiO_2(101) stoichiometric surface under (a) dry conditions and with water adsorbed at (b) 1/8, (c) 3/8 and (d) 6/8 ML coverages. Gray, red and white spheres represent titanium, oxygen and hydrogen, respectively

2. Water Adsorption Energies

In order to analyse the effect of a humid environment on the oxygen vacancy formation energy and the adsorption of TiO_2 nanoclusters, it is fundamental to first understand the effect of the water coverage on the adsorption energy on TiO_2. Adsorption energies are calculated as follows:

$$E_{\text{ads}} = E_{\text{surf+mol}} - E_{\text{surf}} - E_{\text{mol}} \tag{5}$$

Our calculations show that the water adsorption energy on both surfaces strongly depends on the water coverage, with a larger adsorption energy at low coverages, as shown in Tabs. I and II, consistent with previous work in the literature[56, 101, 102]. We found that the water adsorption energy on rutile changes from −1.19 eV to −2.19 eV for 6/8 and 1/8 ML, respectively. On anatase for 6/8 and 1/8 ML coverage we found adsorption energies of −0.61 and −1.46 eV.

Table I: Adsorption energies (in eV per molecule) of H_2O at different coverages on the stoichiometric ("Stoich") and defective rutile TiO_2(110) surface at 1/8, 3/8 and 6/8 ML

	coverages		
Coverage	Stoic.	V_O-I	V_O-I − V_O-II
1/8ML	−2.19	−0.86	−1.13
3/8ML	−1.45	−0.94	−1.06
6/8ML	−1.19	−0.89	−0.98

Table II: Adsorption energies (in eV per molecule) of H_2O at different coverages on the stoichiometric ("Stoich") and defective anatase TiO_2(101) surface at 1/8, 3/8 and 6/8 ML

	coverages		
Coverage	Stoic.	V_O-I	V_O-I − V_O-II
1/8ML	−1.46	−1.14	−1.83
3/8ML	−0.62	−0.61	−0.49
6/8ML	−0.61	−0.48	−0.50

Having calculated the binding energies, we use them to analyse water desorption as a function of the chemical potential of the oxygen in the atmosphere by means of *ab initio* thermodynamics. In this case we consider the system to be in thermodynamic equilibrium with an oxygen and a water (in its gas phase) reservoirs, in order to simulate a realistic humid environment. Surface energies and relative water adsorption energies are then calculated considering the surface in contact with two gas reservoirs, which are both in thermodynamic equilibrium with the surface but not in equilibrium with each other. In this study we consider the chemical potential of the water as independent ($\Delta\mu_{H_2O}$), and we do not consider the components of water molecule (i.e. oxygen and hydrogen) as independent variables. This has been done in order to investigate water desorption as a function of atmospheric temperature and pressure, without considering a complete hydroxylation of the surfaces, see Fig. 15. For a fixed value of the chemical potential of the water we are able to extrapolate the trend of surface energies as a function of the chemical potential of the oxygen. Here the environmental conditions are considered to have a considerable concentration of water in the atmosphere. The limit for the chemical chemical

potential of water molecule in high concentration is −0.91 eV and our calculation are computed in the region right before that value. This condition considers water condensation on a given surface.[62]

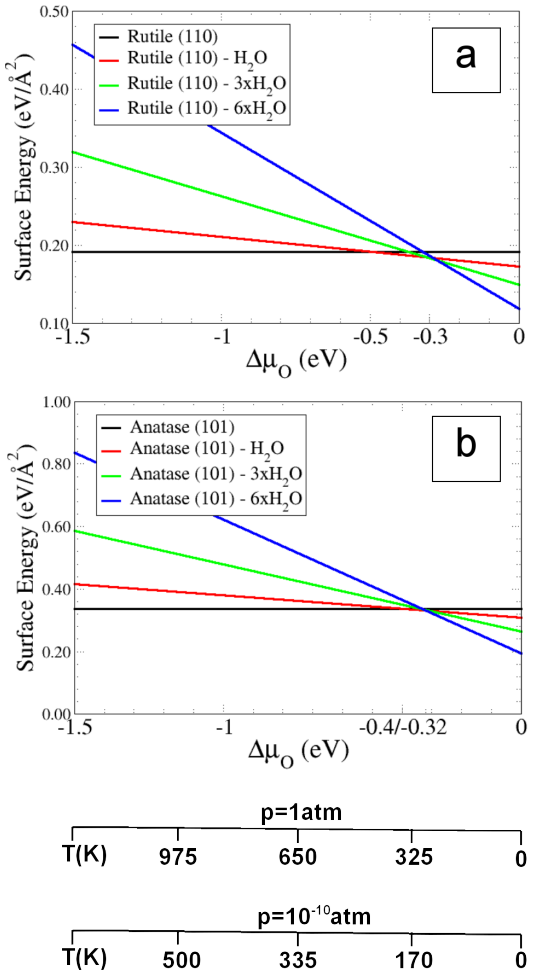

Figure 15: (Color online) Phase diagram of water desorption on rutile (110) (a) and anatase (101) (b) TiO_2 surface, calculated as a function of the chemical potential of the oxygen on the atmosphere.

For rutile (110) surface, we find desorption of all water at $\Delta\mu_O$¿−0.50 eV, when water is abundant in the atmosphere. This would correspond to a temperature of about T≈450K when the atmospheric pressure is p=1atm, while the same value calculated at p=10^{-10}atm becomes T≈250K. There is another transition to be considered. At $\Delta\mu_O$=−0.30 eV we found a transition between high water coverage and low water coverage, namely from 6/8 to 1/8 ML, which means that at p=1atm and p=10^{-10}atm the transition temperatures are T=260K and T=160K, respectively. For anatase (101) total desorption of water at $\Delta\mu_O$=−0.40 eV, which correspond to a temperature of about T≈350K and T≈200K when p=1atm and p=10^{-10}atm, respectively. In

this case the transition from high water coverage and low water coverage occurs at $\Delta\mu_O$=−0.32 eV, which is very similar to the one obtained for rutile ($\Delta\mu_O$=−0.32 eV). Such transitions might become crucial to understand the properties of nanocluster modified surfaces as we discuss in section IV B.

3. Vacancy formation

As previously pointed out, vacancies may be crucial in determining the reactivity of a given surface, not only representing a possible adsorption site, but also actively participating in the reaction (i.e. providing a "source" of electrons available for CO_2 activation). We investigate several vacancy configurations created on the stoichiometric (clean) surface as well as the surface with water adsorbed at different coverages under our DFT+U set-up described in Section 2.
The electronic spin-density (calculated at 0.07 e/$\mathring{A}$) represented in Figs. 16 and 17, for one and two vacancies, respectively, and shows the electron localisation at Ti sites on the rutile (110) surface for the different water coverages, with the typical d-orbital configuration.

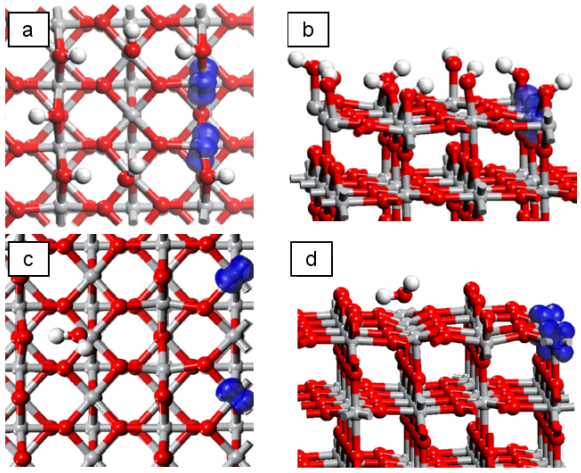

Figure 16: (Color online) Top and side view of spin-desity of rutile TiO_2(110) with one oxygen vacancy at 1/8 ML ((a)and (b)) and 6/8 ML ((c) and (d)) of adsorbed water. Gray, red and white spheres represent titanium, oxygen and hydrogen, respectively, while the blue area shows isosurfaces of spin density, calculated at 0.07 e/$\mathring{A}$

We analyse the vacancy formation energy as a function of the water coverage and we find that it is strongly influenced by the coverage. Vacancy formation energies are calculated as follows:

$$E_{\text{vac}} = E_{\text{surf+vac}} - E_{\text{surf}} - \frac{1}{2}E_{O_2} \tag{6}$$

In our study we did not allow a dissociative adsorption to take place directly on the top of the vacancy site, which mean that the vacancy sites are never occupied by a hydroxyl group. This allows us to isolate and analyse vacancy interaction with atmospheric molecules. Interestingly, different trends in the vacancy formation energy are found on rutile and anatase when one or two vacancies are created in the proximity of a water adsorption site. For rutile (110), with an increase in the water coverage, the single vacancy formation energy increases, while the di-vacancy formation energy decreases (shown in Tab. III). When we introduce the effect of an oxidizing environment, considering the surfaces in equilibrium with an oxygen gas reservoir, this reflects in a phase diagram where the energy of the phase transition from low reduction to high reduction would eventually

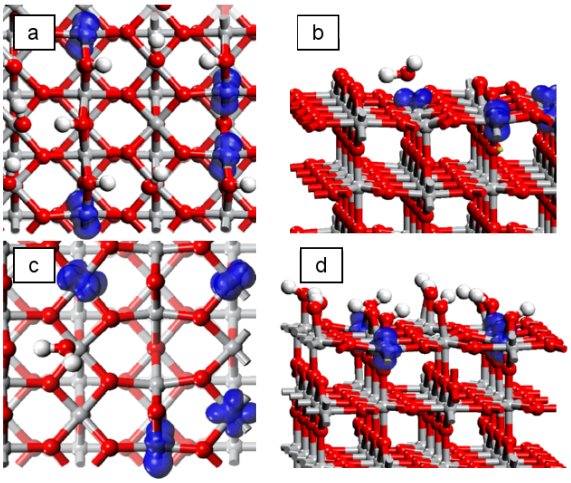

Figure 17: (Color online) Top and side view of spin-desity of rutile TiO_2(110) with two oxygen vacancy at 1/8 ML ((a)and (b)) and 6/8 ML ((c) and (d)) of adsorbed water. Gray, red and white spheres represent titanium, oxygen and hydrogen, respectively, while the blue area shows isosurfaces of spin density, calculated at 0.07 e/$\mathring{A}$

lead to the same value of the chemical potential of oxygen (i.e. $\Delta\mu_O$=−1.42 eV shown in Fig. 18). If we consider the atmospheric pressure to be p=1atm and p=10^{-10}atm, this value corresponds to temperatures T ≈ 1150K and T≈ 700K, respectively. At low water coverage we found the two values, high vacancy density and low vacancy density, to be $\Delta\mu_O$=−1.63 eV and $\Delta\mu_O$=−0.68 eV.

We found a different trend in anatase: with an increase in water coverage, the single vacancy formation energy is only slightly affected with a value between 1.51 eV and 1.56 eV (shown in Tab. IV). Although there is a deviation from the trend for 1/8ML coverage, when the energy becomes larger (i.e. 1.83 eV). on the other hand, the di-vacancy formation energy increases with coverage from 2.16 eV to 2.84 eV. We also found a deviation from the trend when two vacancies are created near a single adsorbed water molecule (1.97 eV).

At high water coverage, the vacancy formation energy on anatase (101) surface is different than rutile (110) surface, with the value of $\Delta\mu_O$=−1.03 eV, corresponding to T ≈ 920K and T≈ 560K, when the atmospheric pressure is p=1atm and p=10^{-10}atm, respectively. Also, for anatase, at low water coverage we found that the two values, high vacancy density and low vacancy density, are relatively close if compared to the rutile surface (i.e. $\Delta\mu_O$=−0.86 eV and $\Delta\mu_O$=−0.60 eV shown in Fig. 19).

Table III: Oxygen vacancy formation energies at different surface water coverages on the rutile TiO_2(110) surface. Adsorption energies are calculated for an isolated (V_O-I) or two close (V_O-I − V_O-II) vacancies, at 0, 1/8, 3/8 and 6/8 ML of water, and the energy is expressed in eV per vacancy.

Coverage	V_O-I	V_O-I − V_O-II
0 ML	1.08	1.69
1/8ML	2.40	1.55
3/8ML	2.60	1.51
6/8ML	2.85	1.41

For both rutile and anatase surfaces the value of $\Delta\mu_O$ at which a single vacancy is formed decreases with increasing water coverage, as shown in Figure 18. Interestingly, we found the opposite trend in the formation of the second vacancy as a function of the chemical potential of the oxygen. When the water coverage increases $\Delta\mu_O$ decreases in rutile but it increases in anatase, as shown in 19. This result indicates a complex interplay

Table IV: Oxygen vacancy formation energies at different water coverages on the anatase TiO_2(101) surface. Adsorption energies are calculated for an isolated (V_O-I) or two close (V_O-I − V_O-II) vacancies, at 0, 1/8, 3/8 and 6/8 ML of water, and the energy is expressed in eV per vacancy.

Coverage	V_O-I	V_O-I − V_O-II
0 ML	1.51	2.16
1/8ML	1.83	1.97
3/8ML	1.55	2.53
6/8ML	1.56	2.84

between water adsorption and vacancy formation in wet conditions that may be important in the photocatalytic activity of TiO_2.

B. TiO_2 Nanocluster Modification of Wet Rutile(110)

Nanocluster modified rutile (110) TiO_2 surfaces have been analysed as described in Section 3. We found that the modified rutile surface can show a smaller band gap after electronic states appear on the top of valence band. This would be extremely beneficial in order to improve the photo-catalytic properties of rutile (110). However, here we want include realistic environmental conditions, which might lead to an extremely different behaviour of the same structure. Here, we consider the adsorption of Ti_4O_8 nanocluster on the wet rutile (110) surface. Two situations are examined: low and high water coverage (4/8 and 6/8 ML). We calculated adsorption energies of the cluster in these conditions to be −5.80 eV and −5.66 eV with a partial hydroxylation of the surfaces. The adsorption energies are higher than that calculated on the dry surface (−3.53 eV), indicating a more stable configuration of the cluster on wet surfaces.[73]

As shown in the previous section, a coverage of water molecules might exist on rutile (110) until high temperatures. However, a different behaviour is apparent for high and low water coverages. As shown in Fig. 20, the analysis of the PEDOS shows a water coverage dependence. While at low water coverage an effect of the NC, which creates new states above the valence band may still exist (albeit smaller than on the dry surface), the same effect completely disappears for a high water coverage, so that there is no red shift in light absorption predicted for this system. The origin of this is due to the NC oxygen atoms that at higher water coverages become hydroxylated due to hydrogen migration from adsorbed water to the TiO_2 nanocluster. By passivating the titanyl oxygen in the nanocluster this removes the high energy VB states originating from the nanocluster pushing them into the VB region.

V. CONCLUSION

By considering the relative energies of electronic states of metal oxides-coupled to TiO_2, we can examine the mechanisms of visible light photocatalytic activity in novel metal oxide modified TiO_2. Figure 21 compares the nano-(left side) and molecular (right side) Fe_2O_3-TiO_2 heterojunction composite structures. In the nano-coupled system, the energy bands of the individual components are unmodified; a similar scenario operates for molecular dye and quantum dot sensitised TiO_2. Upon absorption of visible light, an electron in Fe_2O_3 (band gap of 2.2 eV) is excited. However, the CB-electrons will lie too low in energy to transfer to TiO_2 CB and because the CB minimum of Fe_2O_3 is more positive than the reduction potential of O_2 ($E^0(O_2/O_2^-) = -0.20$

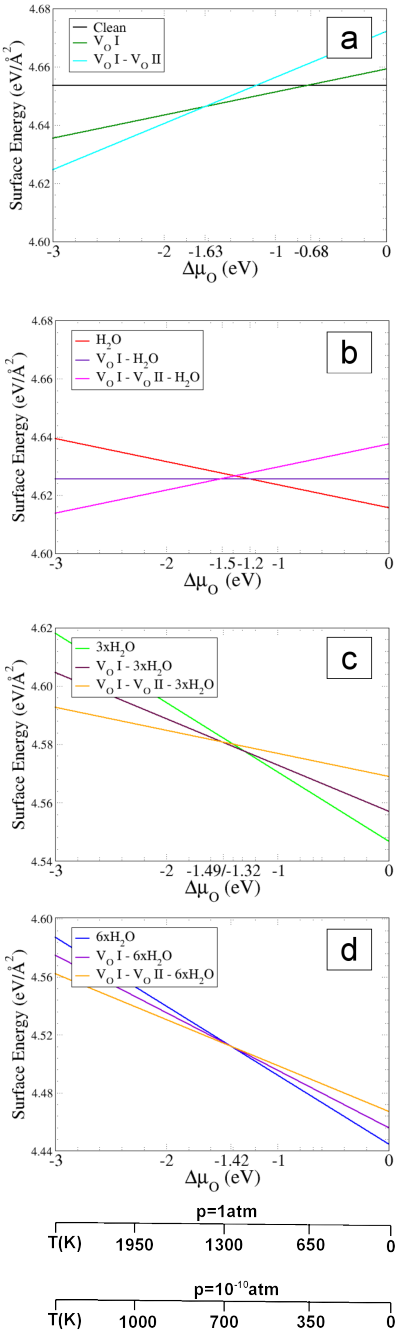

Figure 18: (Color online) Phase diagram of rutile TiO_2(110) stoichiometric (a) and reduced ((b), (c) and (d))surfaces at different water coverages as a function of the chemical potential of atmospheric oxygen.

V, $E_{CB}(Fe_2O_3) = +0.24$ V) the CB electron will ultimately recombine with VB-holes. Thus, while visible light absorption takes place in this nano-coupled system it does not result in visible-light photocatalytic activity. In QD and dye sensitised TiO_2, the sensitizer CB energy is higher than that of TiO_2, and the excited electron transfers from the QD or dye to TiO_2. However, QD- and dye-sensitized TiO_2 can suffer from oxidation and deactivation of the QD or stability issues, which puts limits on the practical use of this materials system in photocatalysis.

In contrast, and this is the significant advantage afforded by molecular scale nanocluster modification of TiO_2, TiO_2 surface modification using molecular-scale metal oxide nanoclusters generally moves the VB-maximum

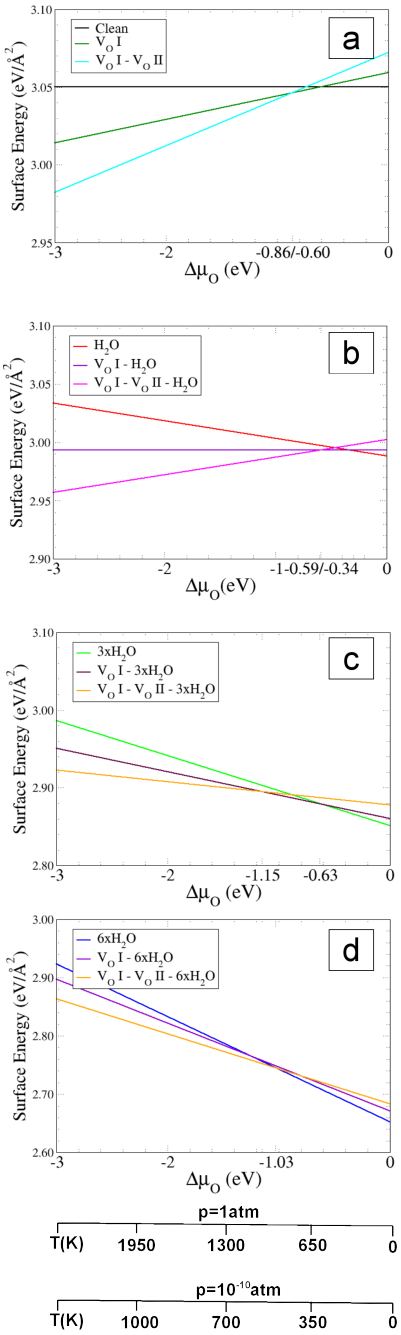

Figure 19: (Color online) Phase diagram of anatase TiO_2(101) stoichiometric (a) and reduced ((b), (c) and (d))surfaces at different water coverages as a function of the chemical potential of atmospheric oxygen.

to higher energy, with no change to the CB-minimum (there are of course systems where the opposite occurs, but the mechanism is the same). The origin of this is as a result of the strong electronic coupling between the nanocluster and the surface through formation of new M-O-Ti interfacial bonds arising from the strong interaction between the MO_x-nanocluster and TiO_2.

An important practical question is that of the stability of the photocatalyst. The experimental work to date on modified TiO_2 [32, 35, 40, 92, 94, 99] indicates good stability of these composite structures under typical experimental conditions. In addition, the study in Ref. [103] indicated good stability of the composite NiO-TiO_2 structure over multiple cycles.

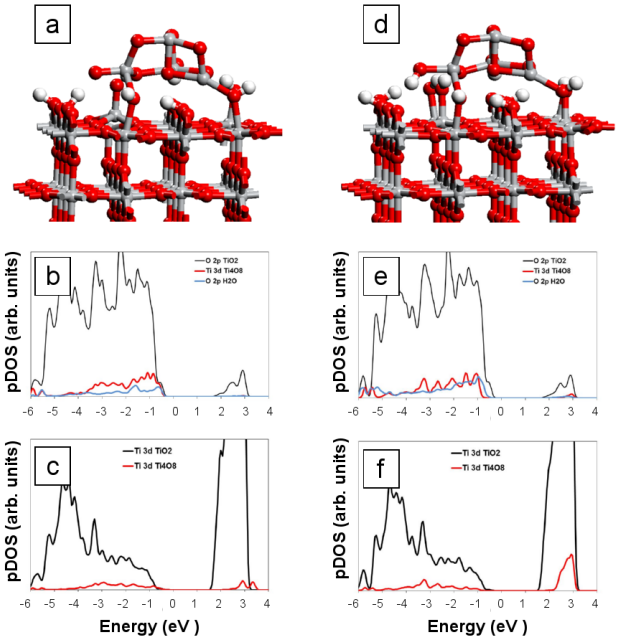

Figure 20: (Color online) TiO_2 nanocluster adsorbed on rutile(110) wet surface and their calculated projected Density of States at water coverage of 4/8 ML ((a), (b) and (c)) and 6/8 ML ((d), (e) and (f)). Here gray, red and white spheres represent titanium, oxygen and hydrogen, respectively. In (b) and (e) the black, red and gray lines represent O_{2p} of the surface, Ti_{3d} of the cluster and O_{2p} of the water on the surface, respectively. In (c) and (f) the black and red lines represent the Ti_{3d} of the surface and cluster, respectively.

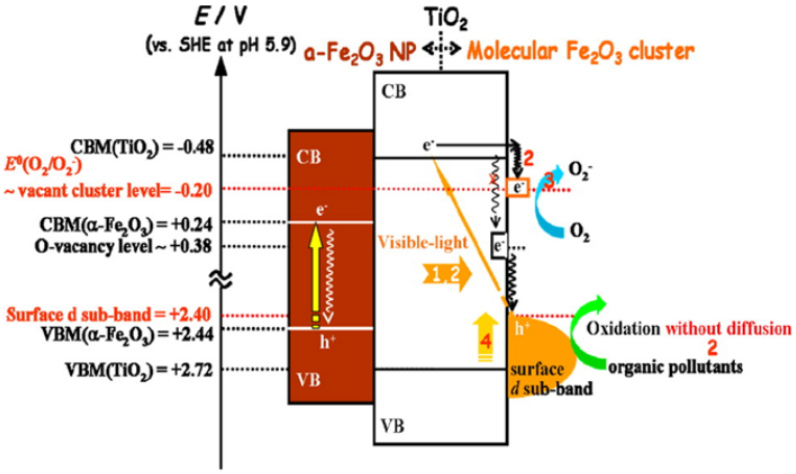

Figure 21: (Color Online) Schematic representation of the nano-scale (left side) and molecular scale (right side) Fe_2O_3-TiO_2 heterojunction composite structures. Reproduced from ref. [32], 2014, with permission from the American Chemical Society

The red shift of light absorption into the visible region, addresses the first major requirement for these photocatalysts. Absorption of visible-light results in electronic excitation from the highest energy occupied, nanocluster derived VB states into the CB states of the TiO_2 support, to generate charge carriers.

The crucial factors in surface modification of TiO_2 by MO_x clusters are as follows: First, from the experimental perspective, precise control of the loading of MO_x clusters on TiO_2 is important to induce visible-light activity. If hole oxidation of a target molecule takes place, e.g. 2-naphthol, then a loading of the oxide nanoclusters that is too high will lower the oxidizing power of the photogenerated holes; this will arise from the upwards shift

in the top of VB, which can be too high so as to reduce the hole oxidising power and reduce the activity. An optimum loading of the oxide nanocluster modifier is therefore present and this depends on the identity of the nanocluster modifier and the targetted molecules.

Second, the DFT simulations indicate that the cluster size (or coverage) affects the catalytic activities of MOs/TiO_2. Third, the effect of surface modification on the photocataltyic activity of TiO_2 can also depend on the crystal form of TiO_2. Grafting of Fe^{3+} ions results in visible-light activity for rutile, but little activity for anatase. In our own work, the surface modification of rutile TiO_2 with SnO_2 clusters increases the UV-light activity, but there is no such effect for modified anatase. Our simulations of model systems show that even though SnO_2 nanoclusters adsorb strongly onto surfaces of both anatase and rutile , the density of states show significant differences between anatase and rutile: on rutile, the CB edge is modified due to new SnO_2 states at the CB edge, increasing light absorption but for anatase, SnO_2 states lie above the TiO_2 CB with no effect as a result of SnO_2 modification. On the other hand, for other metal oxides, such as NiO or PbO, the crystal form of TiO_2 has little effect.

It is well known that the properties of metal oxide nanoclusters in the nm size regime depend on the composition and the number of atoms in the nanocluster and this will impact on the properties of surface modified TiO_2. To explore this in detail requires significant effort to study a wide range of metal oxide nanocluster sizes which is beyond the scope of the work carried out to date. However, in general, for the sub-1 nm diameter nanoclusters we find that once the nanocluster binds to the TiO_2 surfaces, the absorption edge and electronic structure are favourably modified, so that for this size of nanocluster the exact size may not be so crucial in determining the properties of modified TiO_2.

Our first results on the effect of water adsorption at rutile and anatase surfaces show that the stability of different water coverages depends on the crystal form of TiO_2. The formation of oxygen vacancies depends on the crystal form, the water coverage and the vacacy concentration. Particularly interesting from the perspective of nanocluster modified TiO_2 is that for the case of a TiO_2 nanocluster on water-covered rutile the presence of water can entirely kill the effect of the nanocluster modification on the band gap, effectively giving no red shift in light absorption. This is traced back to mobile hydrogen from water migrating to low coordinated oxygen sites, passivating these sites and shifting the corresponding VB states to lower energy.

In summary, combined DFT simulation and experimental work has shown that molecular scale metal oxides of 3d transition metals and d^{10} metals (Sn, Pb) can be formed on TiO_2 rutile and anatase. We have presented insights into the effect of the nanocluster modification of TiO_2 on structure, light absorption and charge carrier localization, giving useful guidelines to enhance the photocataltyic (UV and visible-light) activity of TiO_2, which will be useful for oxidative degradation of organic pollutants or CO_2 reduction. Spectroscopic experiments and DFT simulations have shown that surface modification with MO_x nanoclusters can shift the VB-maximum of TiO_2 to higher energy due to the formation of multiple new interfacial metal-O-Ti bonds; there also are oxides which shift the CB edge upon TiO_2 modification. The interfacial electron transfer accompanied by visible-light absorption enhances charge separation, with hole localization on the nanocluster modifier and electron localization on the TiO_2 support (or vice versa if the CB edge is shifted). This new nanoscale coupling of molecular scale metal oxide nanoclusters and TiO_2 shows great promise as a solar environmental photocatalyst that can be used to purify water and air or to reduce CO_2.

VI. ACKNOWLEDGEMENTS

We acknowledge support from Science Foundation Ireland (SFI) through the Starting Investigator Research Grant Program, project "EMOIN" grant number SFI 09/SIRG/I1620, SFI through the US-Ireland R&D Partnership Program, grant number SFI 14/US/E2915 and the European Commission through the COST Action CM1104 "Reducible Metal Oxides, Structure and Function" We acknowledge access to computing resources at Tyndall provided by SFI and by the SFI and Higher Education Authority funded Irish Centre for High End Computing and the European Commission Partnership in Advanced Computing (PRACE, contracts RI-261557, RI-283493 and RI-312763) for access to the UYBHM Computer at Istanbul Teknik Universitesi and the JUROPA Computer at Forschungszentrum Juelich through the DECI initiative. We are honoured to acknowledge our collaboration with Prof. H. Tada on surface modified TiO_2 and for his valuable insights and discussions into these novel photocatalyst materials and our collaboration with Prof. J. A. Byrne (Ulster) and Profs. K. A. Gray, J. Notestein and E. Weitz (Northwestern) on photocatalytic CO_2 reduction.

[1] Diebold U 2003 *Appl. Phys. A Mater. Sci. Process.* **76** 681–687 ISSN 09478396

[2] Fuerte A, Hernández-Alonso M D, Maira A J, Martínez-Arias A, Fernández-García M, Conesa J C and Soria J 2001 *Chem. Commun.* 2718–2719 ISSN 13597345

[3] Li W 2015 *Phys. status solidi - Rapid Res. Lett.* **9** 10–27 ISSN 18626254

[4] Park H, Park Y, Kim W and Choi W 2013 *J. Photochem. Photobiol. C Photochem. Rev.* **15** 1–20 ISSN 13895567

[5] Hashimoto K, Irie H and Fujishima A 2005 *Jpn. J. Appl. Phys.* **44** 8269–8285 ISSN 0021-4922

[6] Anpo M 2000 *Pure Appl. Chem.* **72** 1787–1792 ISSN 1365-3075

[7] Woan K, Pyrgiotakis G and Sigmund W 2009 *Adv. Mater.* **21** 2233–2239 ISSN 09359648

[8] Zhang H, Chen G and Bahnemann D W 2009 *J. Mater. Chem.* **19** 5089

[9] Liu G, Wang L, Yang H G, Cheng H M and Lu G Q 2010 *J. Mater. Chem.* **20** 831

[10] Pelaez M, N T Nolan J A B, Pillai S C, Seery M K, Falaras P, Kontos A G, Dunlop P S M, Hamilton J W J, J A Byrne K O, Entezari M H and Dionysiou D D 2012 *Appl. Cat. B.* **125** 331

[11] Pillai S C, Stanger U L, Byrne J A, Perez-Larios A and Dionysiou D D 2015 *Chem. Eng. J.* **261** 1

[12] Etacheri V, Di Valentin C, Schneider J, Bahnemann D and Pillai S C 2015 *J. Photochem and Photobiol C: Photochemistry Reviews* **25** 1

[13] Asahi R, Morikawa T, Ohwaki K, Aoki K and Taga Y 2001 *Science* **293** 269

[14] Di Valentin C, Pacchioni G and Selloni A 2004 *Phys. Rev. B* **70** 085116

[15] Di Valentin C, Pacchioni G, Selloni A, Livraghi S and Giamello E 2005 *The Journal of Physical Chemistry B* **109** 11414

[16] Di Valentin C, Finazzi E, Pacchioni G, Selloni A, Livraghi S, Paganini M C and Giamello E 2007 *Chem. Phys.* **339** 44

[17] Long R, Dai Y and Huang B 2008 *The Journal of Physical Chemistry C* **113** 650

[18] Long R and English N 2010 *ChemPhysChem* **11** 2606

[19] Long R and English N 2011 *Appl. Pays. Lett.* **98** 142103

[20] Long R and English N 2010 *The Journal of Physical Chemistry C* **114** 11984

[21] Long R and English N 2011 *ChemPhysChem* **12** 2604

[22] Huy H A, Aradi B, Frauenheim T and Deak P 2012 *J. Appl. Phys.* **112** 016103

[23] Huy H A, Aradi B, Frauenheim T and Deak P 2011 *Phys. Rev. B* **83** 155201

[24] Morgan B J, Scanlon D O and Watson G W 2009 *J. Mat. Chem.* **19** 5175

[25] Umebayashi T, Yamaki T, Itoh H and Asai K 2002 *J. Phys. Chem. Solids* **63** 1909

[26] Di Valentin C and Pacchioni G 2013 *Catalysis Today* **206** 12

[27] Gai Y, Li J, Li S S, Xai J B and Wei S H 2009 *Phys. Rev. Lett.* **102** 036402

[28] Long R and English N J 2011 *Phys. Chem. Them. Phys.* **13** 13698

[29] Luu C L, Nguyen Q T, Ho S T and Nguyen T 2013 *Adv. Nat. Sci.: Nanosci. Nanotechnol.* **4** 035003

[30] Xia Y and Yin L 2013 *Phys.Chem. Chem. Phys.* **15** 18627

[31] Zhang Z, Yuan Y, Liang L, Cheng Y, Shi G and Jin L 2008 *J. Hazard. Mater.* **158** 517

[32] Tada H, Jin† Q, Iwaszuk A, and Nolan M 2014 *J. Phys. Chem. C* **118** 12077

[33] Kontos A I, Likodimos V, Stergiopoulos T, Tsoukleris D S, Falaras P, Rabias I, Papavassiliou G, Kim D, Kunze J and Schmuki P 2009 *Chem. Mater.* **21** 662

[34] Nie X L, Zhou S P, Maeng G and Sohlberg K 2009 *Int. J. Photoenergy* 294042

[35] Tada H, Jin Q and Kobayashi H 2012 *Chemphyschem* **13** 3457–61 ISSN 1439-7641

[36] Kawahara T, Konishi Y, Tada H, Tohge N, Nishii J and Ito S 2002 *Angew. Chem. Int. Ed. Engl.* **41** 2811–3 ISSN 1433-7851

[37] Ahmed A Y, Kandiel T A, Oekermann T and Bahnemann D 2011 *J. Phys. Chem. Lett.* **2** 2461–2465

[38] Prieto-Mahaney O O, Murakami N, Abe R and Ohtani B 2009 *Chem. Lett.* **38** 238

[39] Yoshii M, Kobayashi H and Tada H 2015 *ChemPhysChem* **16** 1846

[40] Tada H, Jin Q, Nishijima H, Yamamoto H, Fujishima M, Okuoka S i, Hattori T, Sumida Y and Kobayashi H 2011 *Angew. Chem. Int. Ed. Engl.* **50** 3501–5 ISSN 1521-3773

[41] Lin X, Li D Z, Wu Q P, Fu X Z and Wang X X 2005 *Chem. J. Chin. Univ.* **26** 727

[42] Kisch H 2013 *Angew. Chem. Int. Ed.* **52** 812

[43] Irie H, Shibanuma T, Kamiya K, Miura S, Yokoyama T and Hashimoto K 2010 *Appl. Catal. B Environ.* **96** 142–147 ISSN 09263373

[44] Yu H, Irie H and Hashimoto K 2010 *J. Am. Chem. Soc.* **132** 6898–9 ISSN 1520-5126

[45] Murakami N, Chiyoya T, Tsubota T and Ohno T 2008 *Appl. Catal. A Gen.* **348** 148–152 ISSN 0926860X

[46] Yu H, Irie H, Shimodaira Y, Hosogi Y, Kuroda Y, Miyauchi M and Hashimoto K 2010 *J. Phys. Chem. C* **114** 16481–16487 ISSN 1932-7447

[47] Tada H 2002 *Encyclopedia of Surface and Colloid Science* ed. a. t. hubbard ed Marcel Dekker (New York)

[48] Galynska M and Persson P 2014 *Energetic Materials* (*Advances in Quantum Chemistry* vol 69) (Elsevier) ISBN 9780128003459

[49] Hahn K R, Tricoli A, Santarossa G, Vargas A and Baiker A 2012 *Langmuir* **28** 1646–56 ISSN 1520-5827

[50] Hussain A, Gracia J, Nieuwenhuys B E and Niemantsverdriet J W H 2013 *ChemCatChem* **5** 2479–2488 ISSN 18673880

[51] Koocher N Z, Martirez J M P and Rappe A M 2014 *J. Phys. Chem. Lett.* **5** 3408–3414 ISSN 1948-7185

[52] Patel M, Sanches F F, Mallia G and Harrison N M 2014 *Phys. Chem. Chem. Phys.* **16** 21002–21015 ISSN 1463-9084

[53] Patel M, Mallia G, Liborio L and Harrison N M 2012 *Phys. Rev. B* **86** 045302 ISSN 1098-0121

[54] Sahoo S K, Nigam S, Sarkar P and Majumder C 2013 DFT study of H2O adsorption on TiO2 (110) and SnO2 (110) surfaces *Solid State Physics* vol 1512 pp 292–293 ISSN 0094-243X

[55] Zhao Z Y 2014 *J. Phys. Chem. C* **118** 4287–4295 ISSN 1932-7447

[56] Selloni A 2010 *J. Mater. Chem.* **20** 10319

[57] Kristoffersen H H, Hansen J O, Martinez U, Wei Y Y, J Matthiesen R S, Bechstein R, Lêgsgaard E, Besenbacher F, Hammer B and Wendt S 2013 *Phys. Rev. Lett.* **110** 146101

[58] Tilocca A and Selloni A 2012 *Journal of Physical Chemistry C* **116** 9114

[59] Shi H, Liu Y C, Zhao Z J, Miao M, Wu T and Wang Q 2014 *J. Phys. Chem. C* **118** 20257–20263 ISSN 1932-7447

[60] Albuquerque A R, Bruix A, Sambrano J R and Illas F 2015 *J. Phys. Chem. C* **119** 4805–4816 ISSN 1932-7447

[61] Fronzi M, Soon A, Delley B, Traversa E and Stampfl C 2009 *J. Chem. Phys.* **131** 104701

[62] Fronzi M, Piccinin S, Delley B, Traversa E and Stampfl C 2009 *Phys. Chem. Chem. Phys.* **11** 9188–9199 ISSN 1463-9084

[63] Kresse G 1996 *Phys. Rev. B* **54** 11169–11186 ISSN 0163-1829

[64] Kresse G 1999 *Phys. Rev. B* **59** 1758–1775 ISSN 1098-0121

[65] Iwaszuk A and Nolan M 2011 *J. Phys. Chem. C* **115** 12995–13007 ISSN 19327447

[66] Lucid A, Iwaszuk A and Nolan M 2014 *Mater. Sci. Semicond. Process.* **25** 59–67 ISSN 13698001

[67] Perdew J P, Jackson K A, Pederson M R, Singh D J and Fiolhais C 1992 *Phys. Rev. B* **46** 6671–6687 ISSN 0163-1829

[68] Morgan B J and Watson G W 2007 *Surf. Sci.* **601** 5034–5041 ISSN 00396028

[69] Di Valentin C, Pacchioni G and Selloni A 2006 *Phys. Rev. Lett.* **97** 166803 ISSN 0031-9007

[70] Finazzi E, Di Valentin C and Pacchioni G 2009 *J. Phys. Chem. C* **113** 3382–3385 ISSN 1932-7447

[71] Di Valentin C, Pacchioni G and Selloni A 2009 *J. Phys. Chem. C* **113** 20543–20552 ISSN 1932-7447

[72] Anisimov V I, Zaanen J and Andersen O K 1991 *Phys. Rev. B* **44** 943–954 ISSN 0163-1829

[73] Nolan M, Iwaszuk A and Gray K 2014 *J. Phys. Chem.* **118** 2789–27900

[74] Ma X, Dai Y, Wei W, Huang B and Whangbo M H 2015 *J. Phys. Chem. Lett.* **6** 1876

[75] Zhu Y, Wei W, Dai Y and Huang B 2012 *Applied Surface Science* **258** 4806

[76] Selloni A and Di Valentin C 2011 *Phys Chem Lett* **2** 2223–2228

[77] Iwaszuk A, Mulheran P A and Nolan M 2013 *J. Mater. Chem. A* **1** 2515–2525 ISSN 2050-7488

[78] Jedidi A, Markovits A, Minot C, Bouzriba S and Abderraba M 2010 *Langmuir* **26** 16232–8 ISSN 1520-5827

[79] Reuter K and Scheffler M 2001 *Phys. Rev. B* **65** 035406 ISSN 0163-1829

[80] Fronzi M, Piccinin S, Delley B, Traversa E and Stampfl C 2014 *RSC Adv.* **4** 12245 ISSN 2046-2069

[81] Iwaszuk A and Nolan M 2011 *Phys. Chem. Chem. Phys.* **13** 4963

[82] Hamad S, Catlow C R A, Woodley S M, Lago S and Mejías J A 2005 *J. Phys. Chem. B* **109** 15741

[83] Shevlin S A and Woodley S M 2010 *J. Phys. Chem. C* **114** 17333

[84] Iwaszuk A and Nolan M 2013 *J. Mater. Chem. A* **1** 6670 ISSN 2050-7488

[85] Iwaszuk A and Nolan M 2013 *Catal. Sci. Technol.* **3** 2000 ISSN 2044-4753

[86] Berardo E, Hu H S, Shevlin S A, Woodley S M, Kowalski K and Zwijnenburg M A 2014 *J. Chem. Theory Comput.* **10** 1189–1199 ISSN 1549-9618

[87] Iwaszuk A, Nolan M, Jin Q, Fujishima M and Tada H 2013 *J. Phys. Chem. C* **117** 2709–2718 ISSN 1932-7447

[88] M Fujishima Q J, Yamamoto H, Tada H and Nolan M 2012 *Chem. Phys. Phys. Chem.* **14** 705–711

[89] Jin Q, Fujishima M, Nolan M, Iwaszuk A and Tada H 2012 *J. Phys. Chem. C* **116** 12621–12626 ISSN 1932-7447

[90] Jin Q, Fujishima M, Iwaszuk A, Nolan M and Tada H 2013 *J. Phys. Chem. C* **117** 23848–23857 ISSN 19327447

[91] Nolan M 2011 *Phys. Chem. Chem. Phys.* **13** 18194–9 ISSN 1463-9084

[92] Jin Q, Fujishima M and Tada H 2011 *J. Phys. Chem. C* **115** 6478–6483 ISSN 1932-7447

[93] Libera J A, Elam J W, Sather N F, Rajh T and Dimitrijevic N M 2010 *Chem. Mater.* **22** 409–413 ISSN 0897-4756

[94] Bhachu D S, Sathasivam S, Carmalt C J and Parkin I P 2014 *Langmuir* **30** 624–630 ISSN 0743-7463

[95] Payne D J, Egdell R G, Walsh A, Watson G W, Guo J, Glans P A, Learmonth T and Smith K E 2006 *Phys. Rev. Lett.* **96** 157403 ISSN 0031-9007

[96] Walsh A, Payne D J, Egdell R G and Watson G W 2011 *Chem. Soc. Rev.* **4455** 4455

[97] Walsh A and Watson G W 2005 *J. Solid State Chem.* **178** 1422–1428 ISSN 00224596

[98] Nolan M 2012 *ACS Appl. Mater. Interfaces* **4** 5863–5871 ISSN 19448244

[99] Boppana V B R, Jiao F, Newby D, Laverock J, Smith K E, Dumas J C, Hutchings G and Lobo R F 2013 *Phys. Chem. Chem. Phys.* **15** 6185

[100] Boppana V B R and Lobo R F 2011 *ACS Catal.* **1** 923–928 ISSN 2155-5435

[101] Sanchez V M, Sued M and Scherlis D A 2009 *J. Chem. Phys.* **131** 174108

[102] Vittadini A, Selloni A, Rotzinger F P and Gratzel M 1998 *Phys. Rev. Lett.* **81** 2954

[103] Tang J, Grampp G, Liu Y, Wang B X, Tao F F, Wang L J, Liang X Z, Xiao H Q, and Shen Y M 2015 *J. Org. Chem.* **80** 2724